NASA

Technical Memorandum 79573

Albedo Enhancement and Perturbation of Radiation Balance Due to Stratospheric Aerosols

Harshvardhan

JUNE 1978

National Aeronautics and
Space Administration

Goddard Space Flight Center
Greenbelt, Maryland 20771

TM 79573

ALBEDO ENHANCEMENT AND PERTURBATION OF RADIATION BALANCE DUE TO STRATOSPHERIC AEROSOLS

Harshvardhan*
Laboratory for Atmospheric Sciences
NASA/Goddard Space Flight Center

June 1978

*National Academy of Sciences - National Research Council
Resident Research Associate

GODDARD SPACE FLIGHT CENTER
Greenbelt, Maryland

ALBEDO ENHANCEMENT AND PERTURBATION OF RADIATION BALANCE DUE TO STRATOSPHERIC AEROSOLS

Harshvardhan*
Laboratory for Atmospheric Sciences
NASA/Goddard Space Flight Center

ABSTRACT

The effect of stratospheric aerosols on the earth's monthly zonal radiation balance is investigated using a model layer consisting of 75% H_2SO_4, which is the primary constituent of the background aerosol layer. The reduction in solar energy absorbed by the earth-atmosphere system is determined through the albedo sensitivity, defined here as the change in albedo per unit mid-visible optical depth of the aerosol layer. The optically thin approximation is used in conjunction with the Henyey-Greenstein phase function for scattering to simplify computations. Satellite derived planetary albedos are used as the frame of reference about which the change in albedo is computed. An infrared radiative transfer model is used to estimate the increased greenhouse effect attributed to the aerosol layer. The infrared heating tends to compensate for the albedo effect in altering the radiation balance. The results indicate that the dominant influence of the thin model stratospheric aerosol layer is an increased reflection

*National Academy of Sciences - National Research Council, Resident Research Associate

of solar energy all over the globe except for the polar-winter region, but the change in the radiation balance is seen to be uniform and small equatorwards of 50°. The largest perturbations occur in the spring and fall in the polar regions with the equator-to-pole radiation balance increasing by 6.5-7.0 W/m^2 for an aerosol mid-visible optical depth of 0.1.

CONTENTS

ILLUSTRATIONS

ILLUSTRATIONS (Continued)

ILLUSTRATIONS (Continued)

TABLES

TABLES (Continued)

ALBEDO ENHANCEMENT AND PERTURBATION OF RADIATION BALANCE DUE TO STRATOSPHERIC AEROSOLS

1. INTRODUCTION

The role of stratospheric aerosols in enhancing the reflection of solar radiation has been investigated recently by numerous authors (Harshvardhan and Cess, 1976; Pollack, et al., 1976; Cadle and Grams, 1975; Pinnick, et al., 1976; Herman, et al., 1976). Model calculations by the above and also by Luther (1976) have shown that the dominant climatic effect of these aerosols is enhanced solar reflection with increased infrared opacity playing a smaller role. However, Herman, et al., (1976) and Luther (1976) have also pointed out that the degree of albedo enhancement is a strong function of the albedo of the underlying surface. Broadly speaking, this underlying surface may be divided into two classes, viz. cloud-free portions of the earth-atmosphere system and the cloudy portion. This classification does not imply a high and low albedo differentiation because the effective albedo of a cloud layer above a snow or ice covered surface may be lower than that of the surface alone (Dave and Braslau, 1975). However, with the above exception, the effective albedo of the cloud-free regions is between 0.15 and 0.3 whereas that of cloudy regions is greater than 0.4. In this discussion, the reflection and absorption in the atmosphere is included in computing the effective albedo, an implicit assumption being that the reflectivity of the atmosphere above the stratospheric aerosol layer may be neglected.

The purpose of the present study is to examine the albedo sensitivity of the earth-atmosphere system to a stratospheric aerosol layer under different assumptions regarding surface and cloud albedos and solar zenith angle averaging procedures. Work to date encompasses a broad range of simplifying assumptions. Harshvardhan and Cess (1976) considered an albedo of 0.3 for the unperturbed earth-atmosphere system. Pollack, et al., (1976) assumed a ground albedo of 0.1 and 50% cloud cover with a detailed radiative transfer scheme to yield aerosol layer perturbations, while Herman, et al., (1976) assigned ground albedos to 10° latitude belts in the Northern Hemisphere with seasonal variations and assumed a 50% cloud cover of reflectivity equal to 0.5. The marked changes in albedo sensitivity obtained by Herman, et al., with changing seasons at high latitudes, due to changes in the mean solar zenith angle and surface albedo, suggests that incorrect inferences may be drawn if global average surface albedos and cloud cover are assumed in computing albedo enhancement.

In this work the albedo of the cloud-free portion of the earth-atmosphere system is presented in 10° latitude belts for each month of the year following the recommendation of Budyko (1974). An empirical relation for the effective cloud reflectivity is derived from calculations of Dave and Braslau (1975). With these two sets of albedos as a base, the global albedo change in the presence of a model stratospheric aerosol layer is computed for climatological cloud cover fractions. The procedure is extended to include the zonal variation of albedo sensitivity by month, based on satellite derived planetary albedos. With the inclusion of the effect of the stratospheric aerosol layer on the infrared radiation leaving the top of the atmosphere, the net energy deficit on a zonal basis is obtained. This quantity may be used as an input to energy-balance climate models used for investigating the climatic effects of stratospheric aerosols.

2. ALBEDO SENSITIVITY

The system albedo, α_p, is commonly expressed as

$$\alpha_p = \alpha_c C + \alpha_s (1 - C) \tag{1}$$

where α_s is the cloud-free or clear sky albedo and α_c the albedo with cloud cover; C is the fractional cloud cover. The expression for α_p may be used on a global basis or for individual latitude belts (Budyko, 1974; Cess, 1976). For the remainder of the text α_p will be used to denote the albedo for each 10° latitude belt, with the hemispheric planetary albedo, A, computed as

$$A = \frac{4}{S} \int_0^{\pi/2} \alpha_p(\phi)\, Q(\phi) \cos\phi \, d\phi \tag{2}$$

where ϕ is the latitude, Q the latitudinal distribution of incoming solar radiation and S the solar constant. The integration of Equation (2) is replaced by a summation over the nine hemispheric latitude belts. The perturbation to this planetary albedo with the introduction of a stratospheric aerosol layer enhancement (as following a major volcanic eruption) is related to the optical depth of the aerosol layer. The albedo sensitivity may be defined as $dA/d\tau$ where the optical depth, τ, is computed at some reference wavelength, usually the mid-visible wavelength of 0.55 μm. Since the stratospheric aerosol layer is optically thin ($\tau \ll 1$), the change in albedo is directly proportional to the change in optical depth and the albedo sensitivity may be written as $\Delta A/\Delta\tau$ (Russell and Hake, 1977). In succeeding sections, models of the planetary albedo and reflectivity of the aerosol layer are postulated and the albedo sensitivity computed.

3. SURFACE AND CLEAR SKY ALBEDO

The fraction of solar radiation incident on a surface that is reflected by it is the surface albedo α_{so}. Using the mean value of albedo for various natural surfaces, Budyko (1974) has suggested appropriate values of land albedos to be used for different climatic and seasonal regimes. The values vary from 0.8 for stable snow cover in high latitudes to 0.13 for steppe and forests. The albedo of a water surface to be used for the ocean fraction of latitude belts has also been given by Budyko based on the work of Sivkov (in Kondratyev, 1975). As there is a strong zenith angle dependence of the direct beam albedo, there is a marked seasonal variation at mid- and high-latitudes. The albedo of both land and ocean change dramatically with snow and ice cover and this seasonal variation must also be incorporated in the computation of global albedo. In the present study, data on snow and ice cover compiled by Curran, et al. (1978) were used to generate the seasonal march of albedo at high latitudes. The surface albedos for land and ocean computed after identifying the surface type and incorporating snow and ice cover are presented in Tables 1 and 2, respectively.

The clear-sky albedo, α_s, is the effective albedo of a cloud-free atmosphere over the land and ocean surface identified by the albedos, α_{so}, given in Tables 1 and 2. It is possible to make a detailed radiative transfer calculation averaged over the solar spectrum to obtain α_s; however, for our purposes, a simple parameterization that takes into account molecular and particle scattering as well as gaseous absorption in the atmosphere is sufficient. One such relation may be obtained from the model of Braslau and Dave (1973) for midlatitude summer water vapor and ozone distributions and an absorbing tropospheric aerosol layer. Choosing their Model C1, the planar reflectivity of a clear sky over a black surface may be written as

$$\alpha_s(R = 0,\theta) = 0.05 + 2.4 \times 10^{-6}\theta^2 + 3.2 \times 10^{-9}\theta^4 \qquad (3)$$

where θ is the solar zenith angle in degrees and R is the reflectivity of the underlying surface. To extend this relation to reflecting surfaces, a multiple reflection model is used which yields (Coakley and Chýlek, 1975; Wiscombe, 1975)

$$\alpha_s(R,\theta) = \alpha_s(R = 0,\theta) + \frac{RT_cT_d}{1 - R\alpha_d(R = 0)} \qquad (4)$$

Table 1

Albedo of Land Surface

Latitude \ Month		J	F	M	A	M	J	J	A	S	O	N	D
N	85	—	—			No Land					—	—	—
	75	—	—	0.80	0.80	0.80	0.50	0.40	0.40	0.50	0.80	—	—
	65	—	0.80	0.80	0.80	0.30	0.20	0.15	0.15	0.15	0.30	0.80	—
	55	0.70	0.70	0.70	0.30	0.15	0.15	0.15	0.15	0.15	0.30	0.70	0.70
	45	0.70	0.70	0.40	0.15	0.15	0.15	0.15	0.15	0.15	0.20	0.40	0.70
	35	0.20	0.20	0.20	0.20	0.20	0.20	0.20	0.20	0.20	0.20	0.20	0.20
	25	0.25	0.25	0.25	0.25	0.25	0.25	0.25	0.25	0.25	0.25	0.25	0.25
	15	0.20	0.20	0.20	0.20	0.20	0.20	0.20	0.20	0.20	0.20	0.20	0.20
N	5	0.10	0.10	0.10	0.10	0.10	0.10	0.10	0.10	0.10	0.10	0.10	0.10
S	5	0.10	0.10	0.10	0.10	0.10	0.10	0.10	0.10	0.10	0.10	0.10	0.10
	15	0.20	0.20	0.20	0.20	0.20	0.20	0.20	0.20	0.20	0.20	0.20	0.20
	25	0.20	0.20	0.20	0.20	0.20	0.20	0.20	0.20	0.20	0.20	0.20	0.20
	35	0.20	0.20	0.20	0.20	0.20	0.20	0.20	0.20	0.20	0.20	0.20	0.20
	45					No Land							
	55												
	65	0.20	0.20	0.40	0.80	0.80	—	—	0.80	0.80	0.40	0.20	0.20
	75	0.80	0.80	0.80	0.80	—	—	—	—	0.80	0.80	0.80	0.80
S	85	0.80	0.80	0.80	—	—	—	—	—	0.80	0.80	0.80	0.80

Table 2

Albedo of Ocean and Sea Ice

Latitude \ Month		J	F	M	A	M	J	J	A	S	O	N	D
N	85	—	—	0.80	0.80	0.80	0.70	0.70	0.70	0.70	—	—	—
	75	—	—	0.80	0.80	0.80	0.70	0.70	0.70	0.70	0.80	—	—
	65	—	0.31	0.28	0.26	0.25	0.22	0.19	0.17	0.17	0.20	0.26	—
	55	0.21	0.18	0.15	0.13	0.11	0.09	0.08	0.08	0.09	0.12	0.17	0.20
	45	0.13	0.10	0.09	0.07	0.07	0.06	0.06	0.07	0.08	0.09	0.12	0.14
	35	0.10	0.09	0.08	0.07	0.06	0.06	0.06	0.06	0.06	0.07	0.09	0.10
	25	0.08	0.07	0.07	0.06	0.06	0.06	0.06	0.06	0.06	0.06	0.06	0.07
	15	0.07	0.06	0.06	0.06	0.06	0.06	0.06	0.06	0.06	0.06	0.06	0.07
N	5	0.06	0.06	0.06	0.06	0.06	0.06	0.06	0.06	0.06	0.06	0.06	0.06
S	5	0.06	0.06	0.06	0.06	0.06	0.06	0.06	0.06	0.06	0.06	0.06	0.06
	15	0.06	0.06	0.06	0.06	0.06	0.07	0.07	0.06	0.06	0.06	0.06	0.06
	25	0.06	0.06	0.06	0.06	0.07	0.08	0.08	0.07	0.07	0.06	0.06	0.06
	35	0.06	0.06	0.06	0.07	0.08	0.10	0.10	0.09	0.08	0.07	0.06	0.06
	45	0.06	0.07	0.08	0.09	0.12	0.14	0.13	0.10	0.09	0.07	0.07	0.06
	55	0.08	0.08	0.09	0.12	0.16	0.18	0.19	0.16	0.13	0.12	0.10	0.07
	65	0.16	0.12	0.15	0.22	0.30	—	—	0.36	0.35	0.34	0.30	0.21
	75	0.70	0.70	0.70	0.80	—	—	—	—	0.80	0.80	0.80	0.70
S	85					No	Water						

where T_c and T_d are the planar and diffuse transmission respectively and α_d $(R = 0)$ is the diffuse or global albedo over a black surface. The atmospheric absorptivity used to compute T_c and T_d has been assumed to be 15% which is an average value based on Braslau and Dave's computations. The variation of absorption with solar zenith angle is not very severe and has been ignored. The results of this model are compared with Braslau and Dave (1973) in Figure 1. The correspondence is excellent for both low and high values of R; the differences are least at the higher zenith angles. The mean solar zenith angle, even at the equator is always greater than 50°. Hence at high latitudes, where R is large due to snow and ice cover, θ is much larger so the parameterization is adequate.

Using the above parameterization, one can generate the clear-sky albedos from surface albedo values and these are given in Table 3. The final column in the table is the insolation weighted mean clear-sky albedo of each latitude belt. This is the value of α_s that should be used in mean annual global energy balance climate models as it is a measure of the total solar radiation reflected back to space by the clear sky portion of each latitude belt on an annual basis. The values of clear sky albedo are compared with the minimum albedo obtained from 29 months of satellite observations by Vonder Haar and Ellis (1975) in Figure 2. Although sampling by various satellites occurred at just one local time during daylight hours, the 29-month set includes late morning, near noon and early afternoon orbits; so the results may be considered to correspond to a mean solar zenith angle.

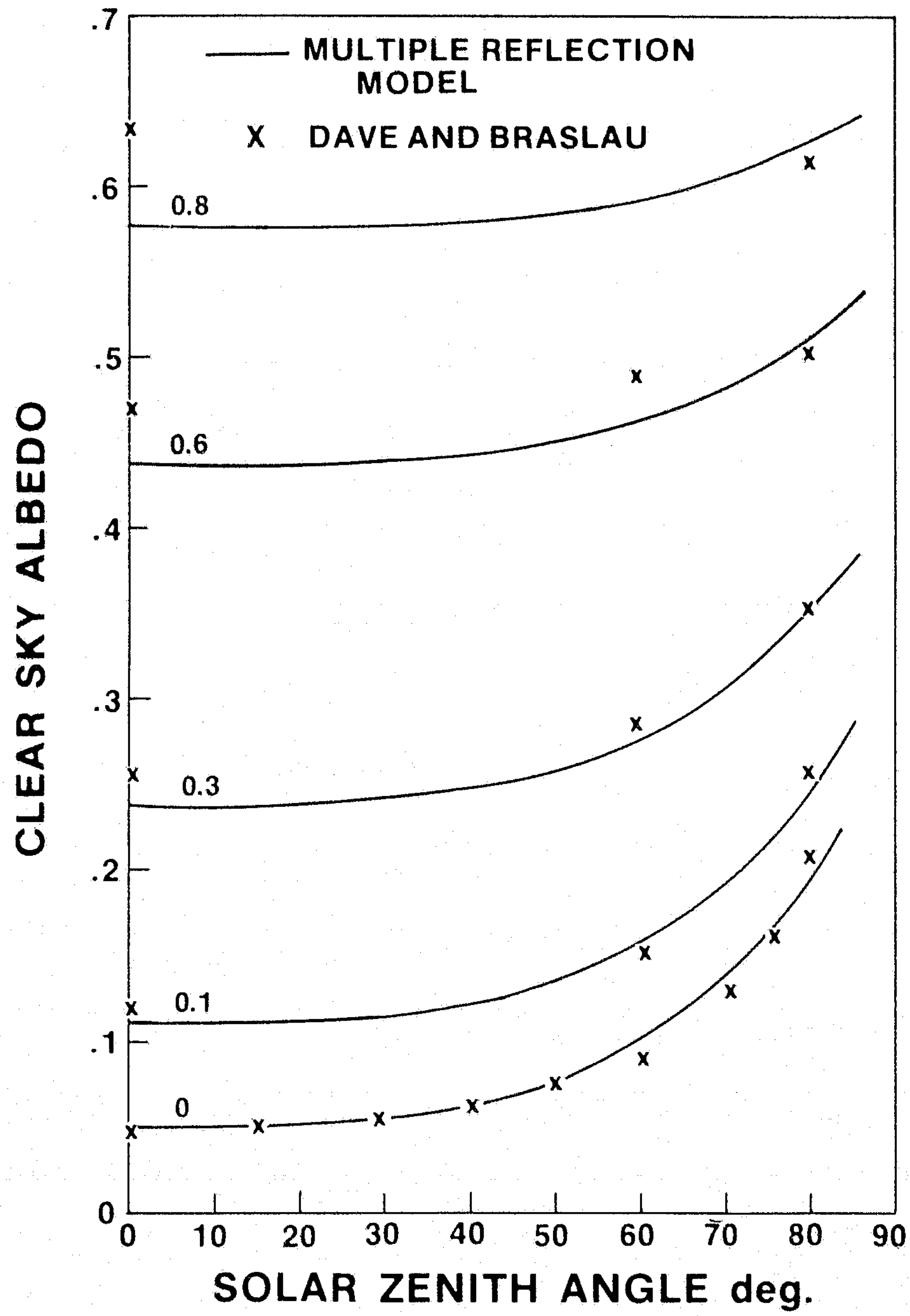

Figure 1. Clear-Sky Albedo Using Multiple Reflection Model Compared with Braslau and Dave (1973) for Surface Reflectivity of 0, 0.1, 0.3, 0.6 and 0.8

Table 3

Cloud-Free Albedos

Latitude \ Month		J	F	M	A	M	J	J	A	S	O	N	D	Insolation Weighted Mean
N	85	—	—	0.64	0.63	0.61	0.54	0.54	0.56	0.58	—	—	—	0.58
	75	—	—	0.63	0.62	0.61	0.50	0.49	0.50	0.54	0.64	—	—	0.54
	65	—	0.55	0.53	0.51	0.28	0.23	0.21	0.21	0.23	0.33	0.56	—	0.30
	55	0.46	0.43	0.40	0.25	0.18	0.17	0.17	0.17	0.19	0.28	0.45	0.46	0.24
	45	0.40	0.37	0.26	0.16	0.15	0.15	0.15	0.15	0.17	0.21	0.30	0.40	0.20
	35	0.22	0.20	0.17	0.16	0.15	0.15	0.15	0.15	0.16	0.18	0.20	0.22	0.17
	25	0.19	0.18	0.17	0.16	0.16	0.16	0.16	0.16	0.16	0.17	0.19	0.20	0.17
	15	0.16	0.14	0.13	0.13	0.13	0.13	0.13	0.13	0.13	0.14	0.15	0.16	0.13
N	5	0.13	0.12	0.12	0.12	0.12	0.12	0.12	0.12	0.12	0.12	0.12	0.13	0.12
S	5	0.12	0.12	0.12	0.12	0.12	0.13	0.13	0.12	0.12	0.12	0.12	0.12	0.12
	15	0.13	0.13	0.13	0.14	0.15	0.16	0.16	0.14	0.13	0.13	0.13	0.13	0.13
	25	0.13	0.13	0.13	0.15	0.17	0.18	0.18	0.16	0.15	0.13	0.13	0.13	0.14
	35	0.13	0.14	0.16	0.18	0.19	0.19	0.18	0.15	0.14	0.12	0.12	0.12	0.14
	45	0.13	0.15	0.18	0.22	0.24	0.23	0.19	0.17	0.14	0.13	0.12	0.12	0.15
	55	0.15	0.15	0.17	0.22	0.28	0.30	0.30	0.25	0.21	0.18	0.16	0.14	0.18
	65	0.21	0.19	0.24	0.34	0.41	—	—	0.41	0.38	0.33	0.28	0.24	0.26
	75	0.59	0.60	0.61	0.64	—	—	—	—	0.63	0.62	0.61	0.58	0.60
S	85	0.61	0.62	0.64	—	—	—	—	—	0.64	0.63	0.61	0.60	0.61

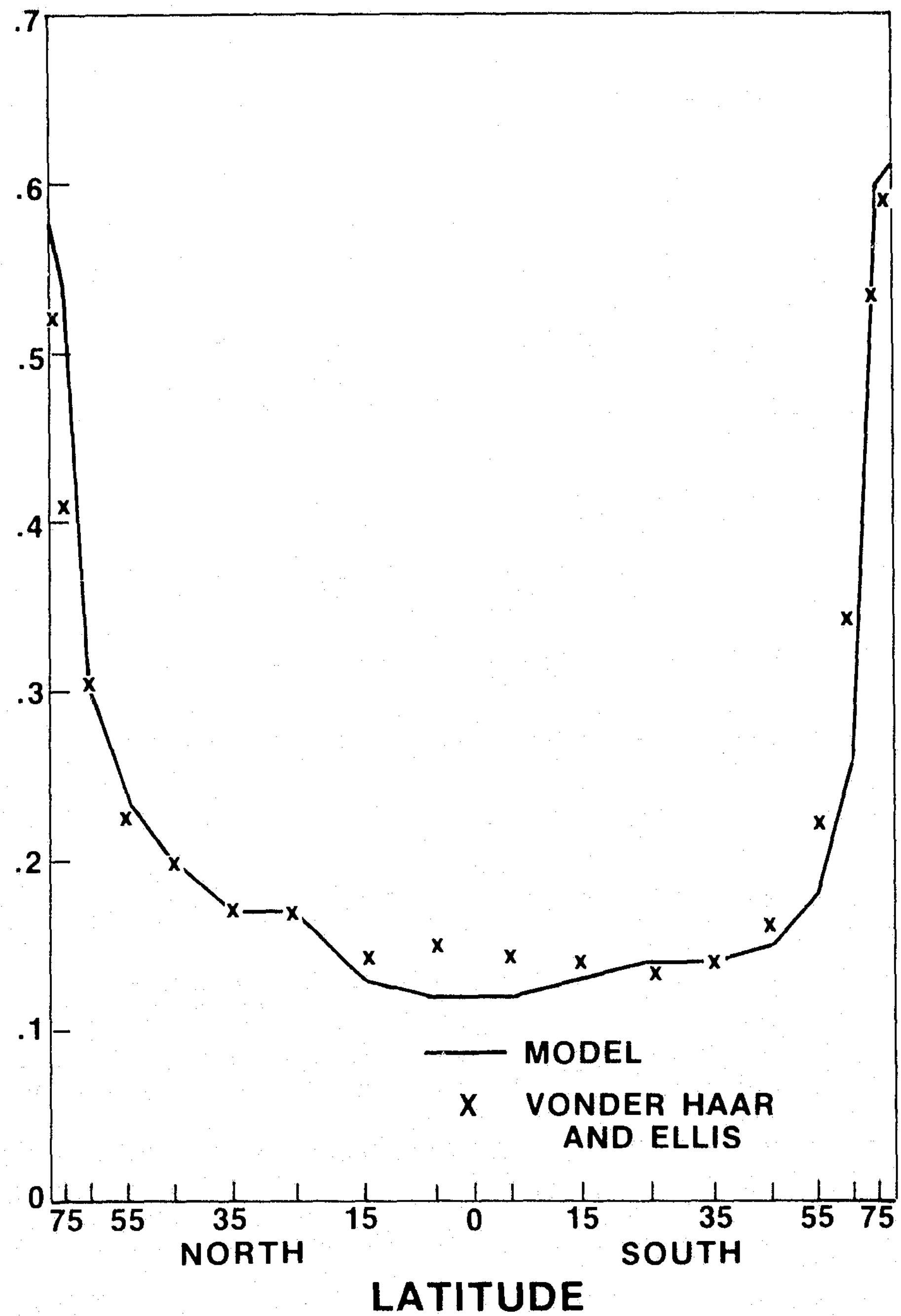

Figure 2. Model Clear-Sky Albedos Compared with Minimum Albedos from Vonder Haar and Ellis (1975)

Viewing geometry and the presence of clouds over snow and ice make observations near the poles unreliable; so only the portion of the globe between latitudes 65°N and S should be considered. Substantial differences between the model and the minimum albedo exist at high latitudes in the Southern Hemisphere and near the Equator. The former is a region of extensive cloudiness (up to 80% average cloud cover; van Loon, 1972), and it is possible there were no totally cloud free satellite viewings recorded, resulting in the 5-10% positive discrepancy. Since the atmospheric model uses one set of radiatively active constituents to represent the whole globe, the parameterization is adequate.

4. CLOUDY-SKY ALBEDO

The spectrally averaged reflectivity of an isolated cloud layer is a function of the physical properties of the cloud and the zenith angle of the incident solar radiation. The albedo of a cloudy sky further depends on the reflectivity of the underlying surface. Since the number of variables involved in specifying a cloud completely for a radiative transfer computation is large and the nature of cloud cover and underlying surface is variable, parameterization of the reflectivity is necessary. In the present work, the cloudy-sky albedo is assumed to depend on the mean solar zenith angle and reflectivity of the underlying surface. An empirical relation between the effective albedo of a cloudy sky over a non-reflecting surface, given by Dave and Braslau (1975) is extended to yield cloudy-sky albedos using a multiple reflection model as in Wiscombe (1975).

Dave and Braslau (1975) have presented results for a detailed atmospheric model with midlatitude summer water vapor and ozone distributions and two tropospheric aerosol concentrations, and also a non-absorbing cloud layer between 3 and 4 km. For parameterization, their model with average aerosols (C1-ST) has been chosen and an excellent fit to the planar reflectivity over a black surface is obtained with

$$\alpha_c(R = 0,\theta) = 0.194 + 4.9 \times 10^{-5}\theta^2 \tag{5}$$

where θ and R have been defined previously. To extend this relation to reflecting surfaces, Equation (4) is used, again with 15% absorption. The results of this model are compared with Dave and Braslau (1975) in Figure 3. Again the parameterization is found to be adequate for the range of R and θ encountered.

The cloud model used by Dave and Braslau has an optical depth of 3.35 at 0.55 μm and a diffuse albedo of 33.2%. This model (henceforth called Model C) has been used to calculate the cloudy-sky albedo, α_c, for each latitude belt and month of the year and is presented in Table 4. The insolation weighted annual mean cloudy-sky albedo is shown in Figure 4 along with the values of α_c deduced by Cess (1976) using satellite measurements of the global albedo and mean annual cloud cover. The model is seen to be an underestimate at all but equatorial latitudes, indicating that the optical depth used in the model is too low. Dave and Braslau (1974) have also presented planar albedos of isolated cloud layers of different optical depths. Choice of an optical depth of 6 and

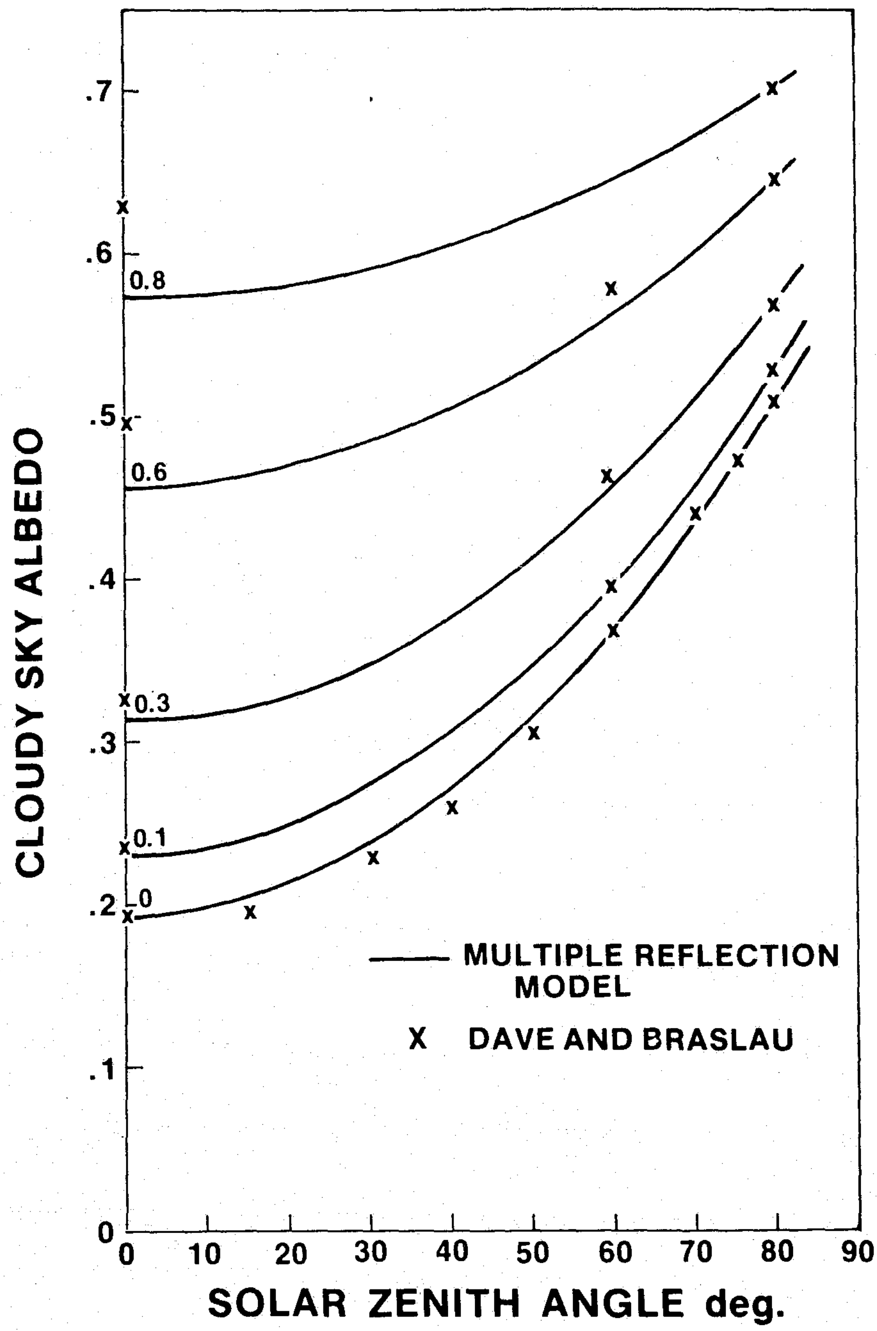

Figure 3. Cloudy-Sky Albedo Using Multiple Reflection Model Compared with Dave and Braslau (1975) for Surface Reflectivity of 0, 0.1, 0.3, 0.6 and 0.8

Table 4

Cloudy-Sky Albedos (Model C)

Latitude	Month	J	F	M	A	M	J	J	A	S	O	N	D	Insolation Weighted Mean
N	85	—	—	0.72	0.70	0.68	0.63	0.65	0.66	0.69	—	—	—	0.66
	75	—	—	0.70	0.70	0.69	0.62	0.62	0.63	0.65	0.72	—	—	0.65
	65	—	0.67	0.64	0.63	0.48	0.46	0.45	0.46	0.49	0.55	0.67	—	0.51
	55	0.62	0.58	0.56	0.46	0.42	0.41	0.41	0.42	0.45	0.51	0.59	0.62	0.46
	45	0.56	0.54	0.47	0.40	0.39	0.38	0.39	0.39	0.40	0.46	0.51	0.57	0.43
	35	0.46	0.44	0.41	0.38	0.38	0.38	0.38	0.38	0.40	0.42	0.45	0.47	0.40
	25	0.43	0.42	0.40	0.38	0.37	0.37	0.37	0.38	0.39	0.42	0.43	0.44	0.40
	15	0.40	0.39	0.37	0.36	0.36	0.36	0.36	0.36	0.37	0.38	0.40	0.41	0.37
N	5	0.38	0.37	0.35	0.35	0.37	0.37	0.37	0.36	0.35	0.35	0.37	0.38	0.36
S	5	0.36	0.35	0.35	0.36	0.37	0.38	0.38	0.37	0.35	0.35	0.36	0.37	0.36
	15	0.36	0.36	0.36	0.38	0.39	0.40	0.40	0.38	0.37	0.36	0.36	0.36	0.37
	25	0.36	0.36	0.37	0.39	0.42	0.43	0.42	0.41	0.38	0.37	0.36	0.36	0.38
	35	0.36	0.37	0.39	0.42	0.44	0.46	0.45	0.43	0.40	0.38	0.37	0.36	0.39
	45	0.38	0.39	0.41	0.45	0.48	0.49	0.49	0.46	0.42	0.40	0.38	0.38	0.41
	55	0.40	0.42	0.44	0.48	0.52	0.54	0.53	0.50	0.47	0.43	0.41	0.40	0.43
	65	0.45	0.45	0.49	0.56	0.60	—	—	0.60	0.56	0.52	0.48	0.47	0.49
	75	0.68	0.69	0.69	0.72	—	—	—	—	0.71	0.70	0.68	0.67	0.66
S	85	0.69	0.70	0.72	—	—	—	—	—	0.73	0.70	0.69	0.68	0.69

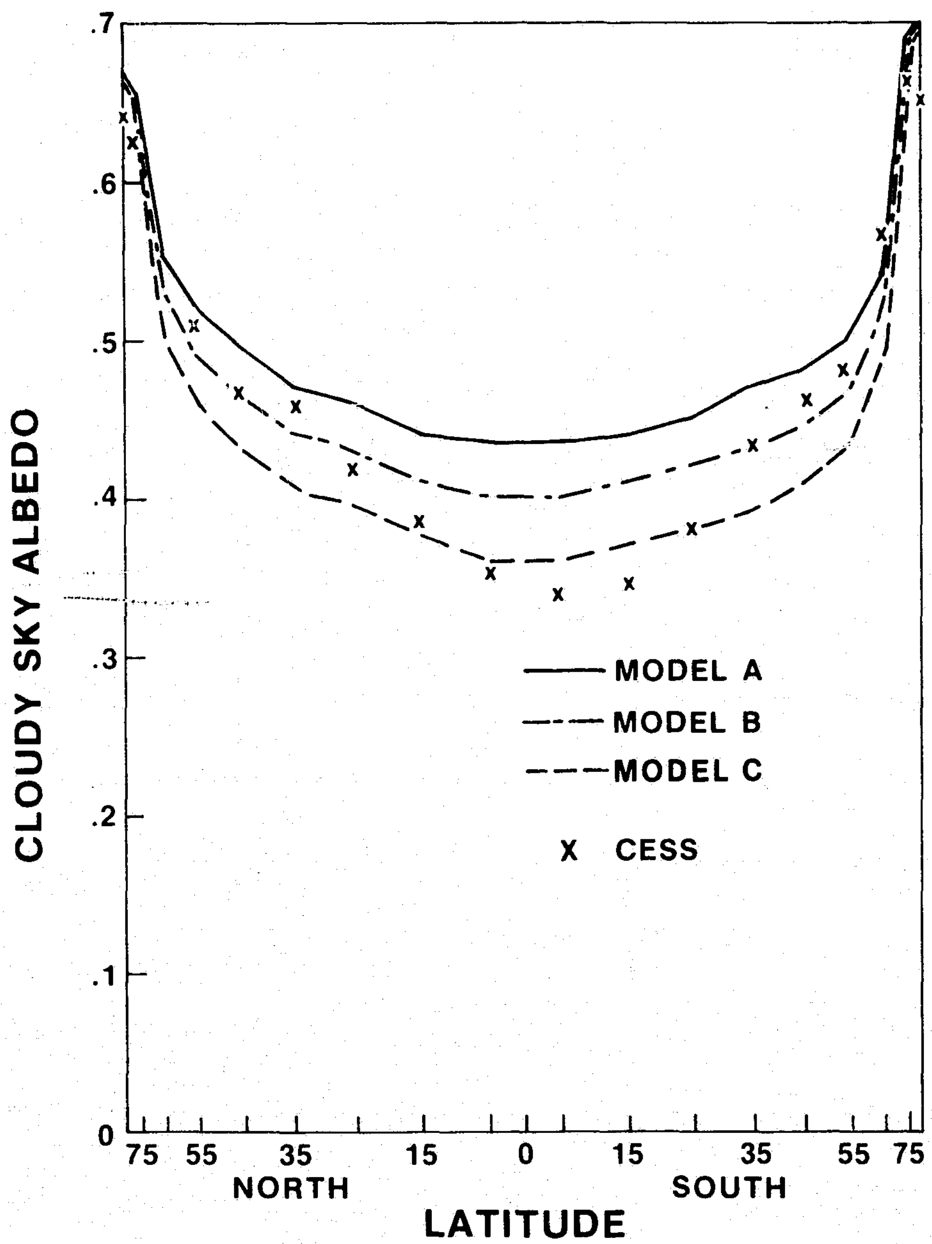

Figure 4. Cloudy-Sky Albedos for Three Models Compared with Values Deduced by Cess (1976)

assumption that the cloud layer is non-absorbing, results in an equation like Equation (5):

$$\alpha_c(R = 0,\theta) = 0.3 + 4.25 \times 10^{-5}\theta^2 \tag{6a}$$

henceforth called Model A. Another model albedo intermediate between that of Equation (5) and Model A is assumed to be

$$\alpha_c(R = 0,\theta) = 0.25 + 4.625 \times 10^{-5}\theta^2 \tag{6b}$$

and is called Model B. The mean annual results have been presented in Figure 4 along with the model given by Equation (5) and Cess (1976).

The highest reflectivity is given by Model A and is seen to be an overestimate throughout while Model B provides good correspondence at mid and high latitudes. The three cloud models have been used in Equation (1) to give the latitudinal distribution of mean global albedo using the clear-sky albedos of Figure 2 and cloud cover fractions, C, from London (1957) for the N. Hemisphere and van Loon (1972) as reported by Cess (1976) for the S. Hemisphere. The results are presented in Figure 5. Also marked are values of α_p from satellite measurements (Ellis and Vonder Haar, 1976) and from the Nimbus-6 ERB experiment (Jacobowitz, et al., 1978). Except for latitudes poleward of 65°, the variation is seen to be simulated quite well by Model B at midlatitude. The N. Hemisphere planetary albedo, A, defined by Equation (2) for the three models is 0.323 for Model A, 0.308 for Model B and 0.291 for Model C.

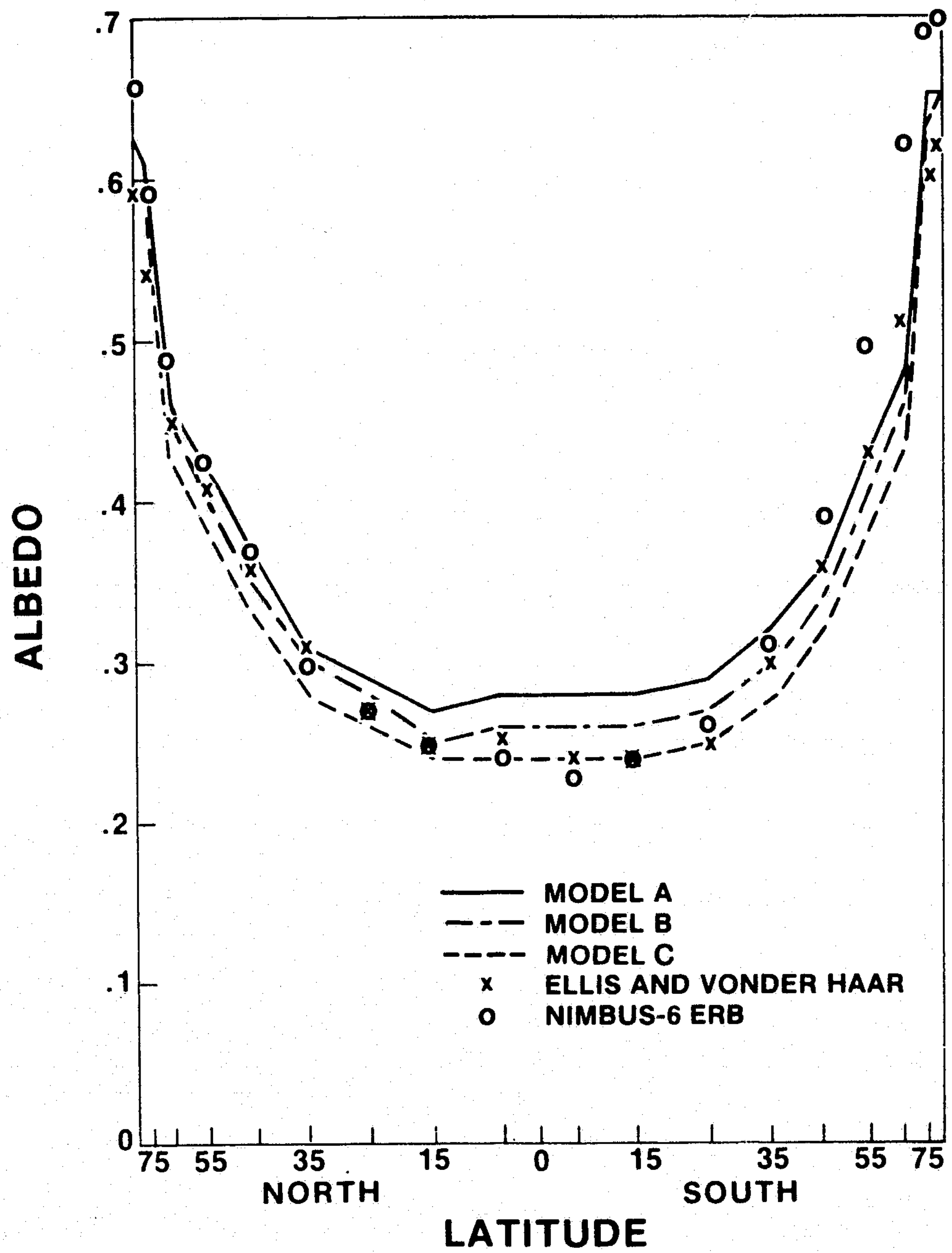

Figure 5. Planetary Albedos Compared with Satellite Derived Results

It may be noted that the planetary albedo derived from the satellite results of Ellis and Vonder Haar is 0.306. The three models are seen to cover the range of reasonable values of the cloudy-sky albedo and the planetary albedo and as such may be used as the basis for computing the albedo sensitivity.

5. STRATOSPHERIC AEROSOL LAYER

There is a persistent tenuous layer of submicron size aerosols in the stratosphere that is composed primarily of an aqueous solution of sulfuric acid. The number concentration of this aerosol layer increases after major volcanic events, and as the residence time of these aerosols is of the order of a year or more, this enhanced concentration persists for up to three years. Recent measurements (Hofmann, et al., 1975; Rosen, et al., 1975) during a period free of major volcanic activity have given a picture of the worldwide distribution of the background stratospheric aerosol layer. For purposes of radiative transfer studies, the quantity of interest associated with the background layer is the optical depth which is 0.005 at 0.55 μm, a value that may be deduced from Hofmann, et al.'s results with an assumption regarding size distribution and refractive index of the aerosols. This illustrates the tenuous nature of the background aerosol layer which may safely be neglected from most atmospheric radiative transfer computations.

Following a volcanic eruption in which the ejected material penetrates into the stratosphere, there is a very significant enhancement of the aerosol layer.

Even after the larger particles that form part of the volcanic debris have fallen back into the troposphere, the aerosols formed from the gaseous ejection remain. Initially this enhanced concentration is limited to the vicinity of the explosion but in a matter of months may spread globally (Dyer and Hicks, 1968). The enhancement of the layer may be 10 or 20 fold in the latitude belt containing the explosion (Volz, 1970) and this can definitely be expected to have radiative effects.

One result of this severe enhancement is the additional reflection of solar energy back to space, and previous work mentioned in Section 1 shows that this indeed is the major radiative effect. However, the magnitude of this effect is crucial in determining the radiative perturbation that may be expected from an enhancement. The albedo sensitivity introduced in Section 2 is a measure of the increased solar reflectivity. A radiative model of the aerosol is needed to compute the reflectivity of the aerosol layer. Mie theory for spherical particles may be used to compute radiative parameters. The aerosol composition is assumed to be 75% H_2SO_4 (Rosen, 1971; optical constants tabulated in Palmer and Williams, 1975) and a modified gamma size distribution (Shettle and Fenn, 1976), normalized to 1 particle/cm^3 is adopted:

$$\frac{dn(r)}{dr} = 324\, r \exp(-18\, r) \tag{7}$$

with dn(r)/dr the number of particles per cm^3 with radii between r and r + dr, where r is in microns. At the mid-visible wavelength of 0.55 μm, the radiative parameters are $\beta_{ex} = \beta_{sc} = 1.1 \times 10^{-4}\ km^{-1}$, $\tilde{\omega} = 1$ and $g = 0.73$ with β_{ex} and β_{sc} the extinction and scattering coefficients respectively, $\tilde{\omega}$ the single scattering albedo and g the asymmetry parameter. The optical depth of a uniform layer of number concentration 1 cm^{-3} is $\tau = \beta_{ex}$ h where h is the height or depth of the layer. A typical background distribution at mid-latitudes is given in Table 5.

6. AEROSOL REFLECTIVITY

As in the case of a cloud deck overlying a reflecting surface, a multiple reflection model may be used to determine the albedo sensitivity of the stratospheric aerosol layer. For this, the reflective property of the isolated aerosol layer has to be determined based on the model introduced in Section 5. Here all computations are made at a wavelength of 0.55 μm; however, radiative properties may be averaged over the solar spectrum. The reflectivity of the layer at 0.55 μm is roughly 25% greater than a solar averaged value (Harshvardhan and Cess, 1976).

Since the optical depth of the background aerosol layer is only 0.005 and even after major volcanic events is normally less than 0.1, the optically thin approximation is used to compute the reflectivity of the layer. In this limit the planar albedo, a, is given by (Coakley and Chýlek, 1975)

$$a(\mu_0) = \frac{\tilde{\omega}\tau}{\mu_0} \frac{1}{2} \int_0^1 d\mu \, p(\mu, -\mu_0) \qquad (8)$$

where τ is optical depth, μ_0 the cosine of the angle of incidence and $p(\mu, \mu')$ is the azimuth independent part of the scattering phase function. The global albedo, $\bar{a}$, is

Table 5

Background Distribution of Stratospheric Aerosols at Mid-Latitudes (based on Shettle and Fenn, 1976)

Altitude, km	β_{ex}, km^{-1} (at $0.55\mu m$)	
	Spring-Summer	Fall-Winter
11	8.0×10^{-4}	6.0×10^{-4} — tropopause location
12	5.5	5.5
13	5.0	5.5
14	4.5 — tropopause location	5.5
15	4.0	6.0
16	4.0	6.5
17	4.5	6.0
18	5.0	5.5
19	5.2	5.0
20	5.3	4.0
21	5.0	3.2
22	3.5	2.7
23	2.5	2.0
24	2.0	1.7
25	1.6	1.4
Total Optical Depth $\tau_{0.55\mu m} = \sum_{12}^{25} \beta_{ex} \Delta h$	0.0054	0.0057

$$\bar{a} = \tilde{\omega}\tau \int_0^1 d\mu \int_0^1 d\mu' \, p(\mu, -\mu') \tag{9}$$

It may be noted that both $a(\mu_0)$ and $\bar{a}$ are directly proportional to the optical depth in this limit. The scattering phase function is computed from the model parameters mentioned in Section 5 and the integrations in Equations (8) and (9) may be carried out for selected solar zenith angles following the procedure of Wiscombe and Grams (1976). The use of the Henyey-Greenstein phase function (Hansen, 1969), which is

$$p_{HG}(\zeta) = \frac{1 - g^2}{(1 + g^2 - 2g\zeta)^{3/2}} \tag{10}$$

where g is the asymmetry parameter and ζ the cosine of the scattering angle, introduces only small errors in flux and is used here because closed form solutions can be obtained for $a(\mu)$ and $\bar{a}$. These are

$$a(\mu_0) = \frac{\tilde{\omega}\tau}{\mu_0}\left\{\tilde{\omega}_0 - \frac{\tilde{\omega}_1}{2}\mu_0 - \sum_{\ell=1}^{\infty} \tilde{\omega}_{2\ell+1} P_{2\ell+1}(\mu_0)\left[\frac{(-1)(-3)(-5)\ldots(-2\ell+1)}{(2\ell+2)(2\ell)(2\ell-2)\ldots.2}\right]\right\} \tag{11}$$

$$\bar{a} = \tilde{\omega}\tau\left\{\tilde{\omega}_0 - \frac{\tilde{\omega}_1}{4} - \sum_{\ell=1}^{\infty} \tilde{\omega}_{2\ell+1}\left[\frac{(-1)(-3)(-5)\ldots(-2\ell+1)}{(2\ell+2)(2\ell)(2\ell-2)\ldots.2}\right]^2\right\} \tag{12}$$

where $\tilde{\omega}_0 = 1$, $\tilde{\omega}_1 = 3g/4$ and $\tilde{\omega}_{2\ell+1} = (4\ell+3)g^{2\ell+1}$ and P_ℓ is the Legendre Polynomial of order ℓ.

The above equations give the reflectivity of an isolated aerosol layer for direct and diffuse solar radiation respectively. This layer is treated as a thin lid covering the earth-atmosphere system in order to compute the albedo sensitivity. An assumption made here is that the reflection from the portion of the atmosphere above the layer is negligible. The altered albedo of the underlying system which is composed of the atmosphere, clouds and land is obtained from the multiple reflection model, Equation (4)

$$\alpha(\mu_0) = a(\mu_0) + \frac{\alpha'(\mu_0)[1 - a(\mu_0)](1 - \bar{a})}{1 - \bar{a}\alpha'(\mu_0)} \tag{13}$$

where $\alpha'(\mu_0)$ is the unperturbed system albedo and $\alpha(\mu_0)$ is the albedo in the presence of the aerosol layer. As there is no absorption in the model aerosol layer at 0.55 μm ($\tilde{\omega} = 1$), $T_c = 1 - a(\mu_0)$ and $T_d = 1 - \bar{a}$. Equation (13) may be applied to each latitude belt and the resulting albedo integrated over each hemisphere using Equation (2), to yield the albedo sensitivity. Each latitude belt is identified with a different mean solar zenith angle, so the planar reflectivity of the layer, $a(\mu_0)$ will be different. Also, land form and cloud cover are variable over the globe, so the radiative perturbation caused by the introduction of an enhanced stratospheric aerosol layer will be latitude dependent. If instead of mean annual averages, seasonal effects are considered, the changing solar zenith angle, cloud cover and land reflectivity will produce a seasonal dependence as was shown by Herman, et al., (1976). In the next section the significance of this latitudinal variation will be discussed in terms of the planetary albedo sensitivity.

7. PLANETARY ALBEDO CHANGES

As mentioned in Section 2, the hemispheric planetary albedo is calculated by integrating the albedo of each latitude belt, α_p, over the hemisphere using Equation (2). The unperturbed zonal albedo, α_p, is calculated using Equation (1) in which mean annual cloud cover fractions may be used. To compute the perturbed planetary albedo, previous authors have used several options. Harshvardhan and Cess (1976) assumed a system albedo of 0.3 to calculate enhanced solar reflectivity; Herman, et al., (1976) allowed for latitudinal variation of surface albedo but assumed 50% cloud cover with a cloud top albedo of 0.5; and Pollack, et al. (1976) assumed a surface albedo of 0.1 and 50% cloud cover with a specified cloud deck between 3 and 6 km. In this study the mean annual cloud cover is not 50% over each latitude zone and the albedos of the cloudy and cloud-free portions of the zone are significantly different and so may be expected to be perturbed to different extents with the addition of a reflecting layer. Moreover, lower latitudes cover more area and have greater insolation over the year, so planetary albedo changes will be weighted in favor of low latitude changes.

Apart from the above, the wide variation in planar reflectivity of the stratospheric aerosols, $a(\mu_0)$, with latitude will be a dominant effect. Table 6 gives the planar albedo for model aerosol layers with two scattering phase functions at the annual mean solar zenith angle corresponding to the different latitude belts. Owing to the forward bias of the phase function with $g = 0.73$, the planar albedo

Table 6

Albedo of Aerosol Layer

Latitude	Cosine of Mean Solar Zenith Angle	$a(\mu_0)/\tau$	
		g = 0.726	g = 0
N 85°	0.257	1.045	1.946
75°	0.274	0.941	1.825
65°	0.316	0.739	1.582
55°	0.385	0.520	1.299
45°	0.453	0.384	1.104
35°	0.513	0.302	0.975
25°	0.560	0.254	0.893
15°	0.592	0.227	0.845
N 5°	0.609	0.214	0.821
	$\frac{\bar{a}}{\tau}$	0.401	1.0

is much less than that for the isotropic phase function. Also, there is a much wider variation with latitude. The effect of latitude on the albedo sensitivity may be illustrated by using Equation (13) to compute the change in the albedo of the underlying system for arbitrary unperturbed system albedos. This is presented in Figures 6 and 7 for a non-absorbing aerosol layer with an asymmetric phase function (g = 0.73) and an isotropic phase function (g = 0) respectively. The ordinate is the albedo sensitivity, here

$$\frac{\alpha(\mu_0) - \alpha'(\mu_0)}{\tau}$$

and $\alpha'(\mu)$ is the unperturbed system albedo. Results are presented for direct beam radiation at the solar zenith angles corresponding to different latitudes and for diffuse radiation. Two features may be noted from these figures. For g = 0.73, the albedo sensitivity for latitudes equatorward of 45° is less than that

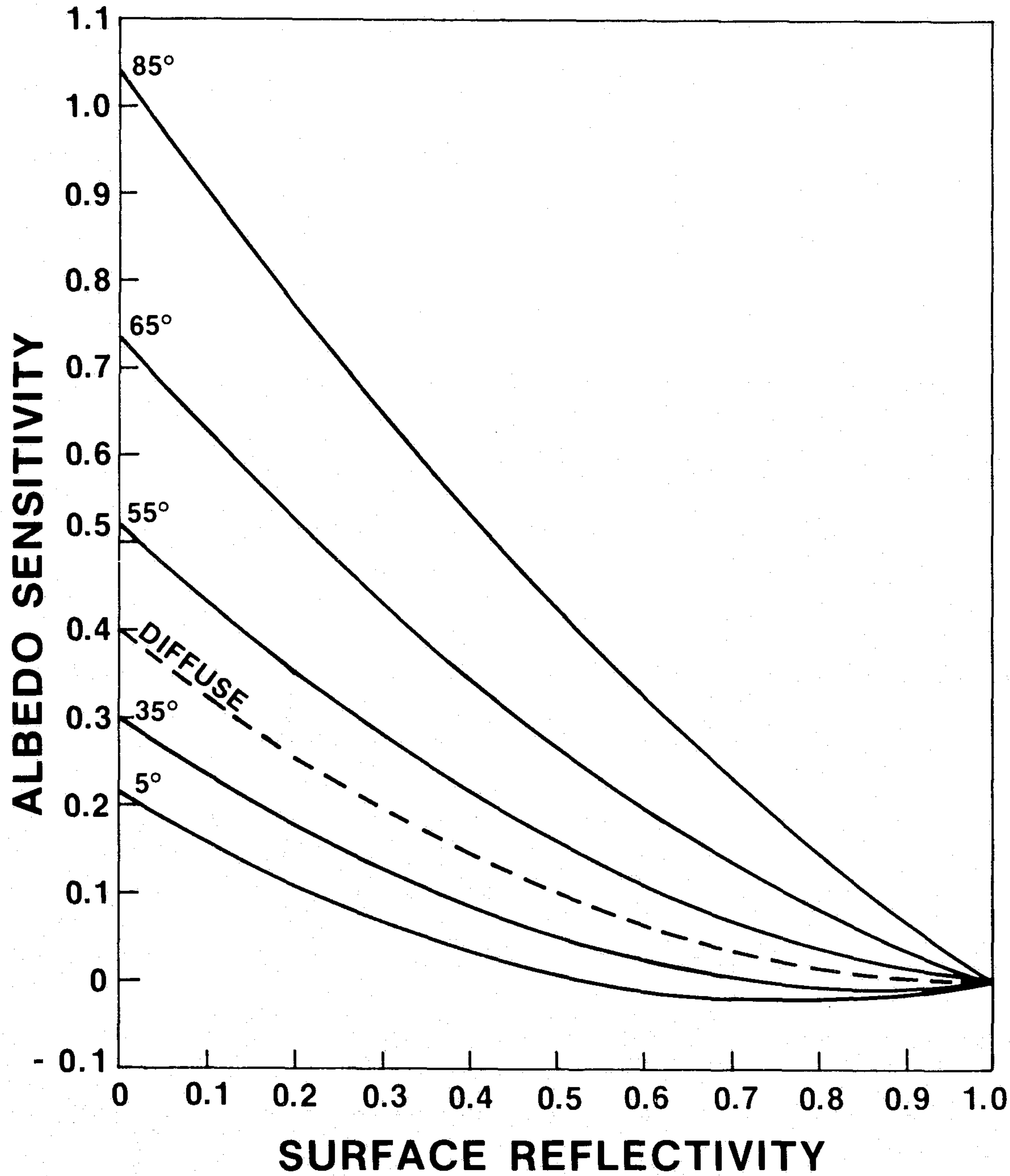

Figure 6. Albedo Sensitivity for Model Aerosol Layer with g = 0.73 for Direct-Beam Radiation at Annual Mean Solar Zenith Angles Corresponding to Latitudes 85°, 65°, 55°, 35°, 5°, and for Diffuse Radiation

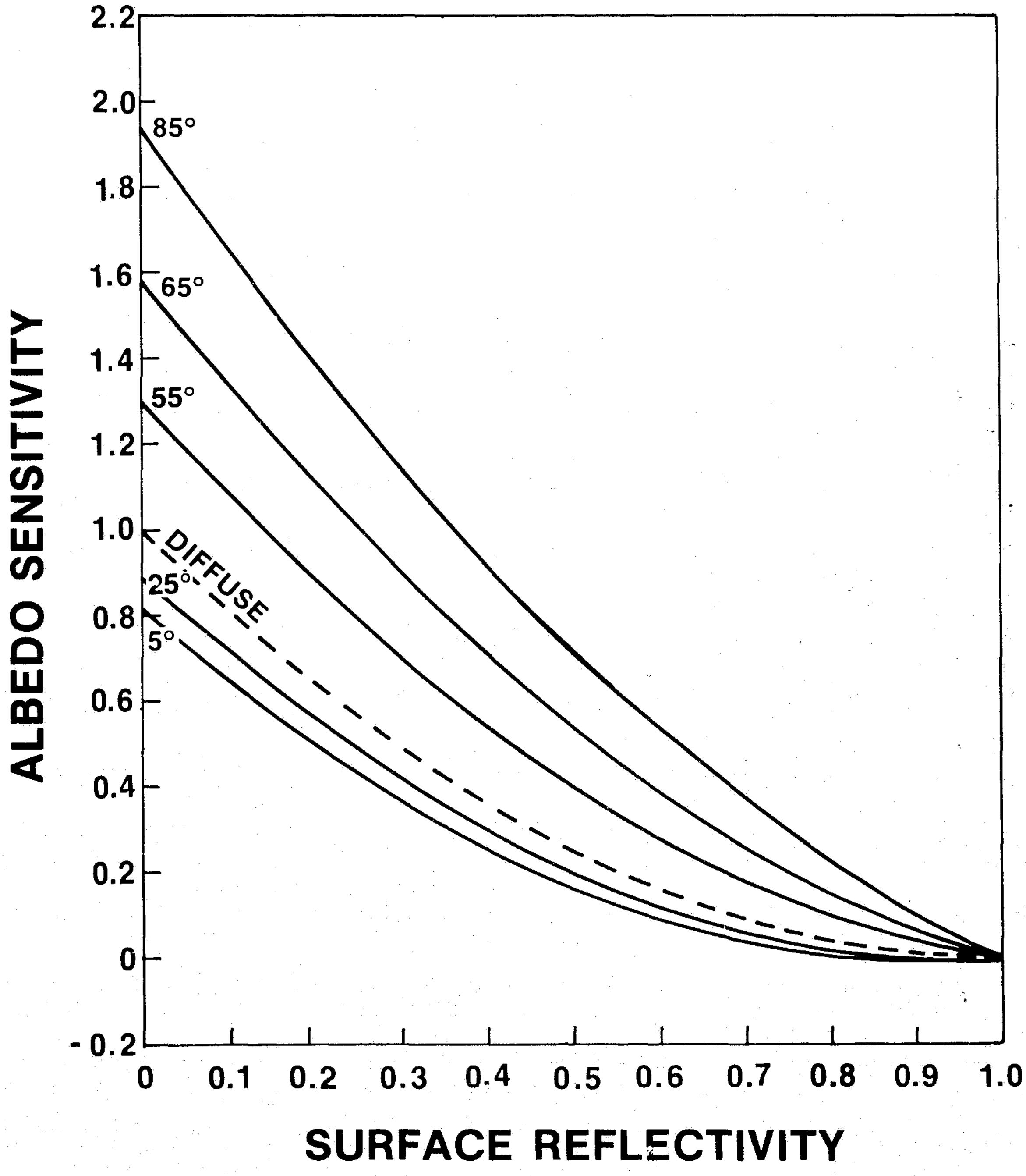

Figure 7. Same as Figure 6 Except with g = 0 (Isotropic Scattering)

for diffuse radiation. These latitude belts contain over 70% of the surface area and receive more solar insolation than regions poleward of 45°. This explains some of the discrepancies in planetary albedo sensitivity obtained by using different averaging procedures as described later. The other notable feature is the almost linear relationship between the albedo sensitivity and surface reflectivity at high latitudes. This feature is present in the case of slightly absorbing aerosols as shown in Figure 8 in which results at two mean solar zenith angles corresponding to 85° N and 5° N latitude are presented for $\tilde{\omega}$ = 0.99, 0.95 and 0.9.

Here three methods of estimating planetary albedo changes are compared. For a particular set of albedos, α_s and α_c, and cloud cover fraction C, the planetary albedo is computed. Now it is assumed that a uniform optically thin layer of aerosol covers the planet. Using the multiple reflection model, the new system albedo is

$$A_{new} = \bar{a} + \frac{A_{old}(1 - \bar{a})^2}{1 - \bar{a} A_{old}} \tag{14}$$

Note that the diffuse or Bond albedo of the stratospheric layer, $\bar{a}$, has been used, which for the present model is 0.4τ, such that the albedo sensitivity is

$$\frac{A_{new} - A_{old}}{\tau} = \frac{0.4(1 - A_{old})^2}{1 - 0.4\tau A_{old}} \approx 0.4(1 - A_{old})^2 \tag{15}$$

when $\tau \ll 1$. This is a hemispheric annual averaging procedure. Another approach is to compute the change in reflectivity of each latitude belt with constant cloud cover. This is a zonal annual average accomplished by applying the reflection scheme to each α_p and then integrating over the hemisphere using Equation (2). The change in planetary albedo is then

$$A_{new} - A_{old} = \frac{4}{S}\int_0^{\pi/2} (\alpha_{p,new} - \alpha_{p,old})Q\cos\phi\, d\phi \qquad (16)$$

where, for each latitude belt

$$\alpha_{p,new}(\phi) = a(\phi) + \frac{\alpha_{p,old}(1-\bar{a})[1-a(\phi)]}{1-\bar{a}\alpha_{p,old}} \qquad (17)$$

with ϕ the latitude. The zenith angle dependence of the planar reflectivity has been translated to a latitude dependence. The mean annual solar zenith angle has been chosen for this purpose.

The zonal annual average computation may also be carried out separately for the cloudy and clear sky portions of the atmosphere. Here the multiple reflection model takes the form

$$\alpha_{c,s,new}(\phi) = a(\phi) + \frac{\alpha_{c,s,old}(1-\bar{a})[1-a(\phi)]}{1-\bar{a}\alpha_{c,s,old}} \qquad (18)$$

and

$$\alpha_{p,new} - \alpha_{p,old} = (\alpha_{c,new} - \alpha_{c,old})C + (\alpha_{s,new} - \alpha_{s,old})(1-C) \qquad (19)$$

The three methods of computing the albedo sensitivity have been carried out for the clear sky albedos and the three model cloudy albedos given in Figures

Table 7

Mean Annual Albedos and Cloud Cover Fractions

Latitude	Cloud Fraction	α_s	α_c		
			Model A	Model B	Model C
N 85°	0.55	0.58	0.67	0.67	0.66
75°	0.61	0.54	0.66	0.65	0.65
65°	0.64	0.30	0.56	0.53	0.51
55°	0.64	0.24	0.52	0.49	0.46
45°	0.57	0.20	0.50	0.47	0.43
35°	0.47	0.17	0.47	0.44	0.41
25°	0.41	0.17	0.46	0.43	0.40
15°	0.44	0.13	0.44	0.41	0.38
N 5°	0.51	0.12	0.44	0.40	0.36
S 5°	0.50	0.12	0.44	0.40	0.36
15°	0.47	0.13	0.44	0.41	0.37
25°	0.47	0.14	0.45	0.42	0.38
35°	0.54	0.14	0.47	0.43	0.39
45°	0.65	0.15	0.48	0.45	0.41
55°	0.79	0.18	0.50	0.47	0.43
65°	0.77	0.26	0.54	0.52	0.49
75°	0.56	0.60	0.69	0.69	0.66
S 85°	0.47	0.61	0.70	0.69	0.69

Table 8

Albedo Sensitivity

Models	Planetary Albedo		Albedo Sensitivity $\Delta A/\Delta\tau$					
			Hemispheric Annual Average		Zonal Annual Average (Cloudy & Clear Combined)		Zonal Annual Average (Cloudy & Clear Separate)	
	N. H.	S. H.	N. H.	S. H.	N. H.	S. H.	N. H.	S. H.
Model A	0.323	0.327	0.184	0.182	0.123	0.123	0.132	0.133
Model B	0.308	0.309	0.192	0.191	0.130	0.132	0.137	0.139
Model C	0.291	0.289	0.202	0.203	0.138	0.142	0.143	0.147
Cess	0.306	0.301	0.193	0.196	0.132	0.136	0.138	0.140

2 and 4 respectively. The mean annual albedos and cloud cover fractions from London (1957) and van Loon (1972) for the N and S Hemispheres respectively are given in Table 7. The hemispheric albedo sensitivity calculated using the three methods are listed in Table 8 along with the unperturbed planetary albedo for the three different cloud models and also for albedo values deduced by Cess (1976) from satellite derived results in Ellis and Vonder Haar (1976).

The results of the albedo sensitivity computation are significant in two ways. First, there is a substantial reduction in the sensitivity when a zonal average is taken instead of a hemispheric average. The mean value of this reduction is 31% for the four cases considered. This lower value is a more appropriate measure of the mean annual planetary albedo sensitivity to a uniform stratospheric aerosol perturbation. The explanation for this reduction may be found in Table 6 and Figure 6. The planar reflectivity of the aerosol layer is a very strong function of the zenith angle and the use of hemispheric averaging is equivalent to assuming a diffuse reflectivity which is greater than the planar reflectivity for mean solar zenith angles corresponding to latitudes equatorward of 45°. The increased reflectivity of the layer in polar regions is compensated by the effect of lower latitudes which have more area and receive more solar insolation. If the aerosol scattering had been isotropic this effect would not have been as pronounced. Again from Table 6 and Figure 7, it is evident that the planar reflectivity for isotropic scattering is nearly uniform till 35° latitude and is very close in value to the diffuse reflectivity. An example is a computation as presented in Table 8 for isotropic scattering. Using the parameters of Model B for the Northern Hemisphere, the albedo sensitivity is 0.480 with hemispheric averaging and 0.465 with zonal averaging (0.482 when cloud and cloud-free albedos are taken separately).

The other feature of the results is the insignificant change in albedo sensitivity when cloudy and clear sky portions of each latitude zone are considered separately. This may seem surprising because the albedo sensitivity is a strong function of the reflectivity of the underlying surface as is shown in Figure 6. However, the relationship is monotonic and nearly linear for the higher latitudes; the same is true for lower latitudes when the underlying system albedo is less than 0.5. The effective albedo of a partly cloudy area lies between the cloudy and clear-sky albedos, the exact value depending on the cloud cover fraction, C, Equation (1). Owing to the near linearity of the albedo sensitivity relationship, the value obtained by considering cloudy and clear-sky portions separately and considering an effective zonal albedo are very nearly the same. The significance of this result is that it is not essential to know the exact cloud cover fraction and cloudy and clear-sky albedos to compute the albedo sensitivity in this case. This argument holds for slightly absorbing aerosols as well, as show shown in Figure 8. Satellite measurements of effective zonal albedos are available by month in 10° latitude belts (Ellis and Vonder Haar, 1976) and present ERB studies are geared to obtaining this information. Therefore it is possible

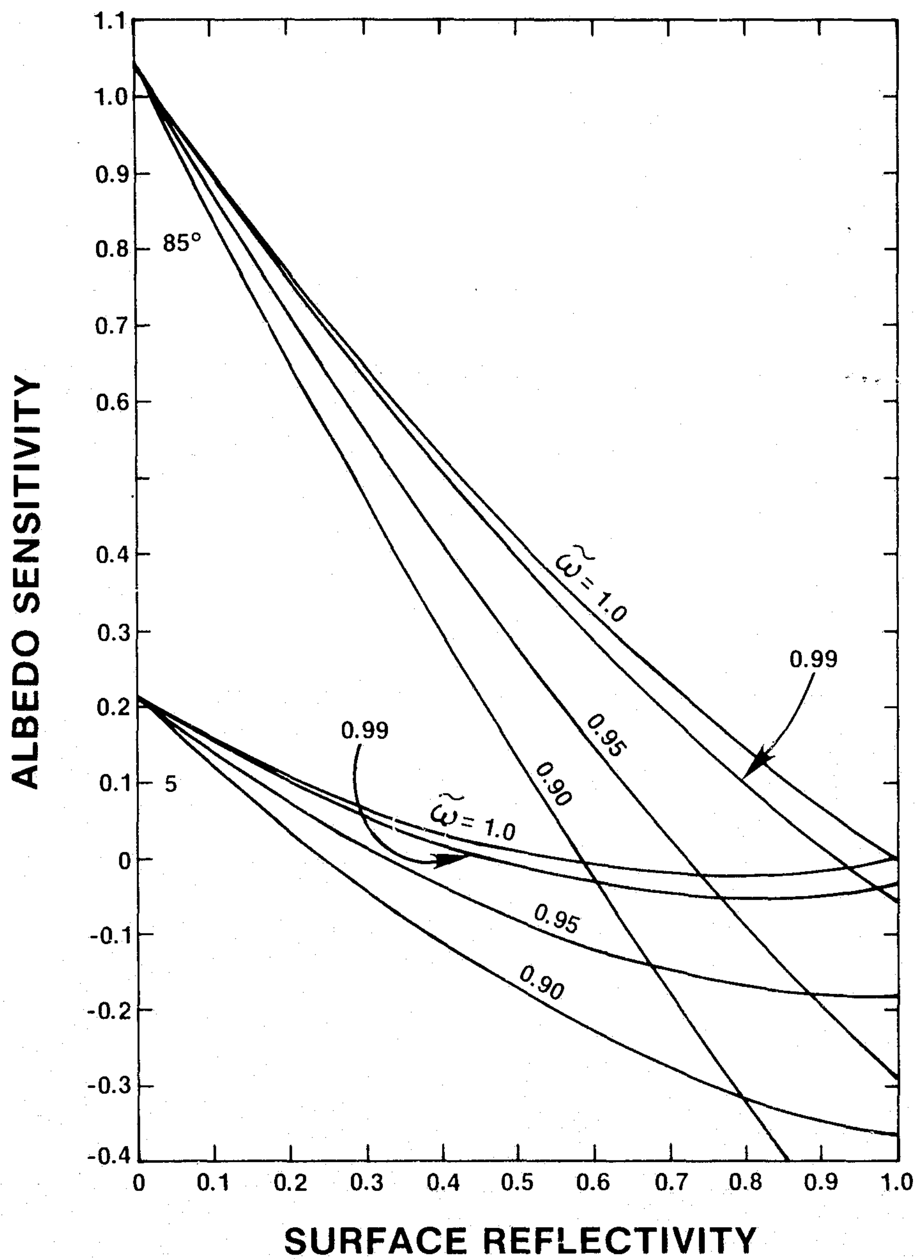

Figure 8. Same as Figure 6 Except for only 85° and 5° Latitude with $\tilde{\omega} = 1.0$, 0.99, 0.95 and 0.9

to estimate the albedo sensitivity of different latitude zones over the annual cycle with current data.

8. MONTHLY ALBEDO SENSITIVITY

The procedure for computing the monthly albedo sensitivity is similar to the annual case. The unperturbed zonal albedo, α_{old}, is taken to be the mean monthly values quoted in Ellis and Vonder Haar (1976). By the discussion in the previous section, we need not take into account the cloudy and cloud-free portions of the zone separately. The reflectivity of the aerosol layer, $a(\mu_0)$, is a function of the solar zenith angle, the variation of which must be included in the computation. To simplify matters, the 21st day of each month has been chosen to compute the reflectivity which has been averaged over the zenith angles made by the path of the sun on that day for the mid-point of each latitude belt. The albedo perturbation caused by the presence of a non-absorbing stratospheric aerosol layer of incremental optical thickness, $\Delta\tau$, will then be $(\alpha_{new} - \alpha_{old})$ where α_{new} is given by Equation (17). With the assumption that the optical depth at 0.55 μm (denoted by τ_{vis}) is representative of the aerosol layer, the albedo sensitivity, $\Delta\alpha/\Delta\tau$, obtained from Equation (17) has been plotted in Figure 9.

The isopleths in Figures 9 and 10 are in units of change of albedo per unit change in optical depth or alternately, the change in albedo in percent of incident solar energy for an optical depth perturbation of $\Delta\tau = 0.01$. The dominant feature is seen to be the zenith angle dependence translated here in a monthly and latitudinal dependence. Over high latitudes the effect of surface reflectivity

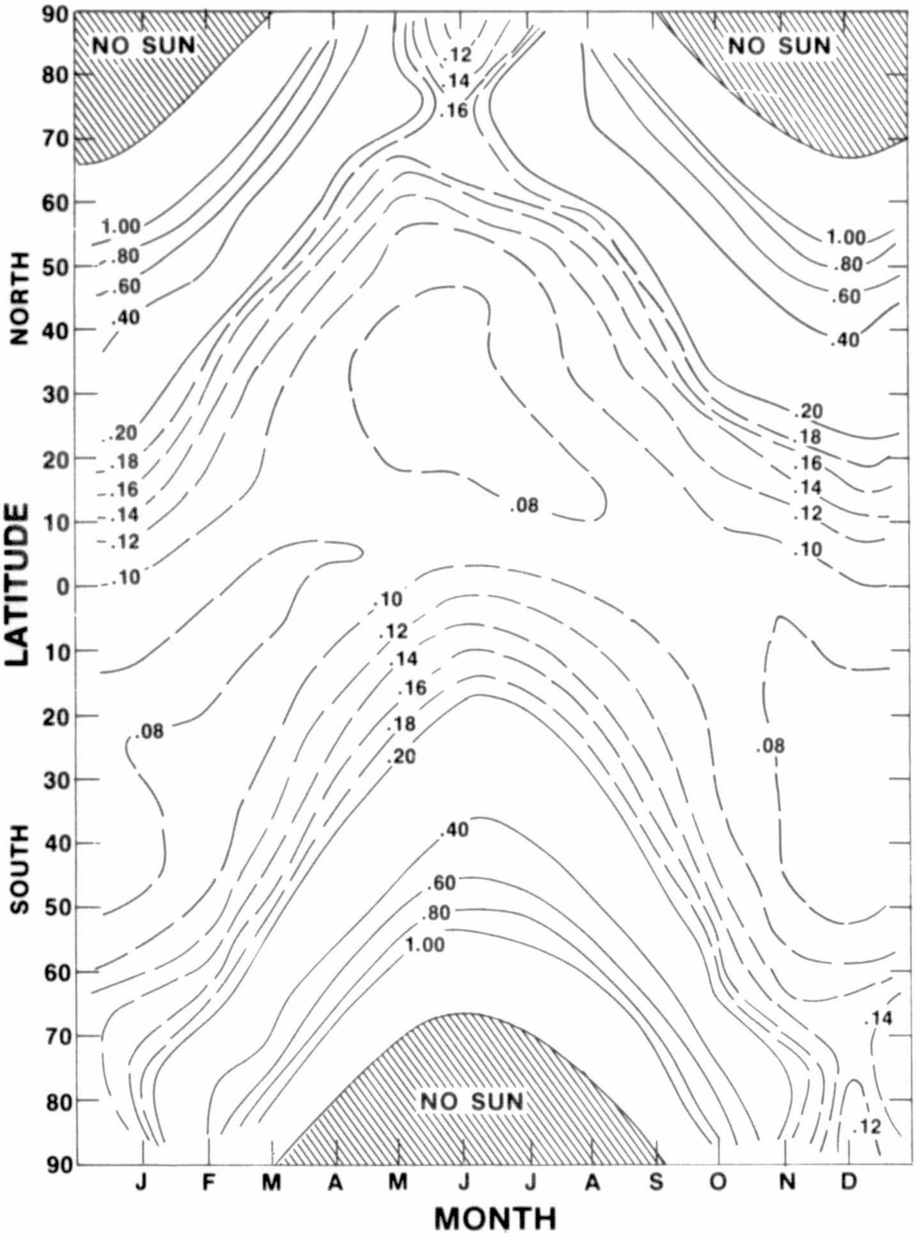

Figure 9. Monthly Zonal Albedo Sensitivity Using Model Reflectivity at 0.55 μm

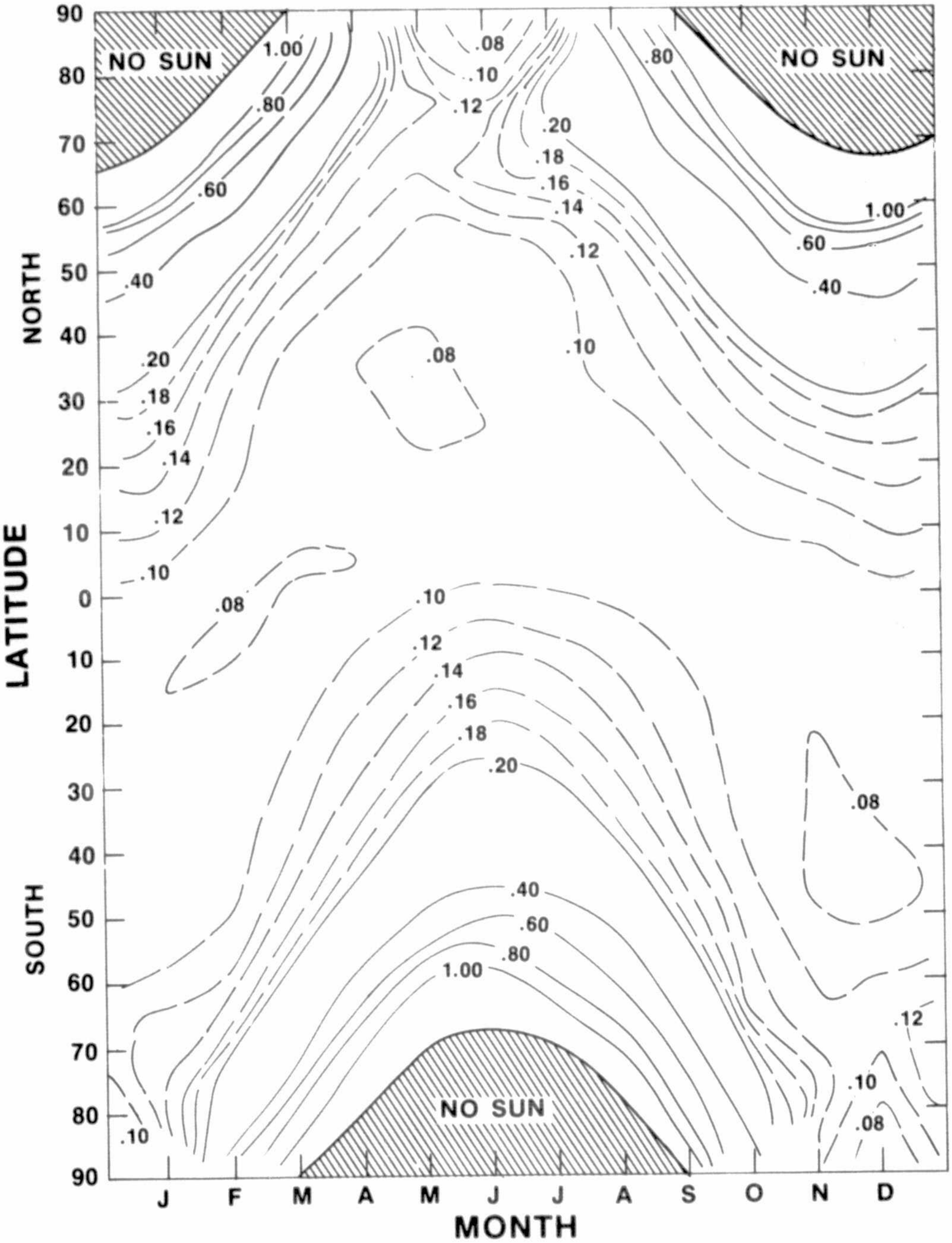

Figure 10. Same as Figure 9 Except with Solar Averaged Reflectivity

may also be noticed, such as the lower values of $\Delta\alpha/\Delta\tau$ in late winter and early spring when there is snow cover on the ground. This phenomenon has been discussed in Section 7 with the help of Figure 6. Figure 10 is a plot of the solar averaged albedo sensitivity which is obtained by repeating the computations carried out at 0.55 μm at a number of wavelengths and taking a weighted mean. The aerosol considered here is slightly absorbing in the solar infrared and Equation (17) may be rephrased in terms of the transmission as

$$\alpha_{new} = a + \frac{\alpha_{old} T\overline{T}}{1 - a\alpha_{old}} \tag{20}$$

where T is planar and $\overline{T}$ is spherical transmission.

These figures may be compared with Figures 5 and 11, respectively, of Herman, et al. (1976) who have plotted the change in albedo in percent for a stratospheric aerosol perturbation optical depth of 0.03 at 0.5 μm. Their results are for the Northern Hemisphere for a prescribed surface albedo variation which assigns values of the albedo according to three classes of surface (bare ground, open water and ice or snow). Clouds are assumed to cover 50% of the area and are simulated by results corresponding to a ground albedo of 0.5. Their results for non-absorbing aerosols show very clearly the high-latitude regions of minimum albedo sensitivity in spring and maximum albedo sensitivity in the fall. Their results for 75% H_2SO_4 averaged over solar wavelengths correspond quite closely to Figure 10 presented here except for high

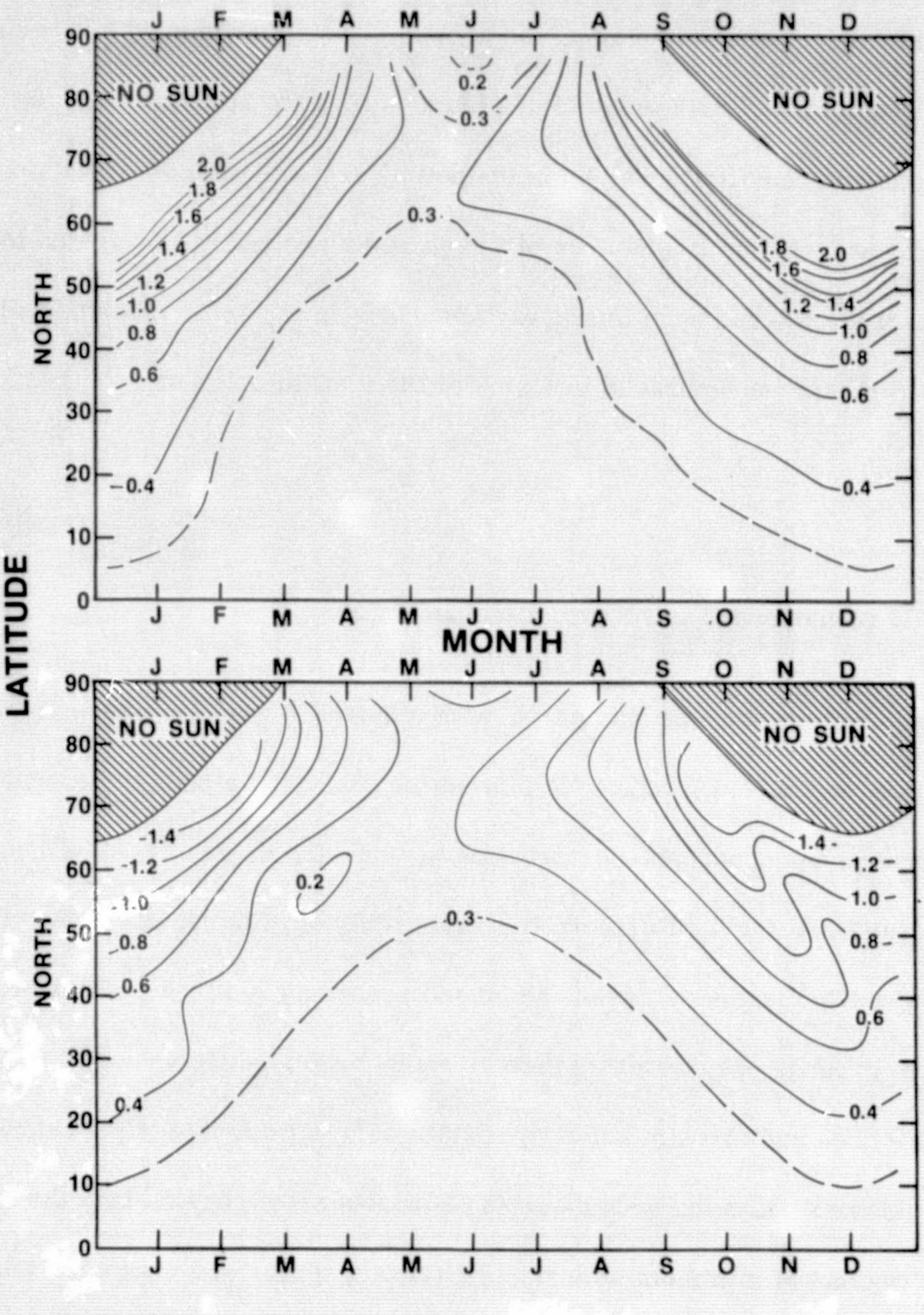

Figure 11. Change in System Albedo in Percent with Addition of Aerosol Layer of Optical Depth 0.03 at 0.5 μm; Present Model (Above) and Herman, et al. (1976) (Below)

latitude regions in the spring and fall. The comparison is facilitated by replotting Figure 10 for the Northern Hemisphere for an optical depth of 0.03 at 0.5 μm. This is shown in Figure 11 in which Figure 11 of Herman, et al., (1976) has been reproduced below for comparison. (It should be noted that the scattering phase function used in their work is slightly different from the one used here.) One reason for the discrepancy is the low values of albedo for high latitude regions quoted by Ellis and Vonder Haar (1976), who recognize that their results are quite uncertain in the 70°- 90° latitude range.

9. RADIATION BALANCE AND CLIMATE MODELING

The annual and monthly zonal albedo sensitivity results have important implications in energy-balance climate modeling. The sensitivity of these models is usually related to perturbations in the magnitude of the solar constant. For example, both Sellers (1969) and Budyko (1969) refer to an increase in volcanic dust loading and a decrease in the solar constant interchangeably. However, even a uniform dust layer of global extent will not lead to a uniform reduction in the solar energy received by a column of the earth-atmosphere system below the stratospheric layer. The computations presented here have shown how this reduction is distributed in latitude and with season. The basic equation of zonal energy balance on an annual mean basis is (Budyko, 1969)

$$Q(\phi)[1 - \alpha(\phi)] - I(\phi) = D(\phi) \tag{21}$$

where $Q(\phi)$ is the solar insolation at latitude ϕ, $\alpha(\phi)$ the albedo, $I(\phi)$ is the outgoing terrestrial infrared radiation and $D(\phi)$ is the divergence of heat. The presence of a stratospheric aerosol layer modifies α through increased reflectivity and I through an increased greenhouse effect acting in the opposite direction. The reduction in solar energy absorbed, $Q\Delta\alpha$, caused by a uniform stratospheric layer of $\tau_{vis} = 0.1$ is plotted in Figure 12 which follows from Figure 10 and the distribution of $Q(\phi)$ for each month.

The net loss in a column of the earth-atmosphere system, however, is $Q\Delta\alpha - \Delta I$, which is the change in the radiation balance and it is necessary to compute the infrared greenhouse sensitivity of the aerosol layer. This is done using an atmospheric radiation model similar to the one by Harshvardhan and Cess (1978) in which an emissivity formulation has been used to calculate the infrared flux. Water vapor and carbon dioxide are considered to be the gaseous absorbers in the atmosphere and a 4 km thick layer of the model aerosol layer is added to determine the enhanced greenhouse effect. The computations have been carried out for the model atmospheres given by McClatchey, et al., (1971) for clear skies and a cloudy sky with cloud top at 6.5 km. The aerosol layer was positioned to correspond to the observed level of peak concentration at different latitudes (Rosen, et al., 1975). Results are presented in Table 9 in which the infrared greenhouse sensitivity is expressed in $(W/m^2)/\tau_{vis}$ and is seen to be a maximum in the tropics and a minimum for the subarctic winter model.

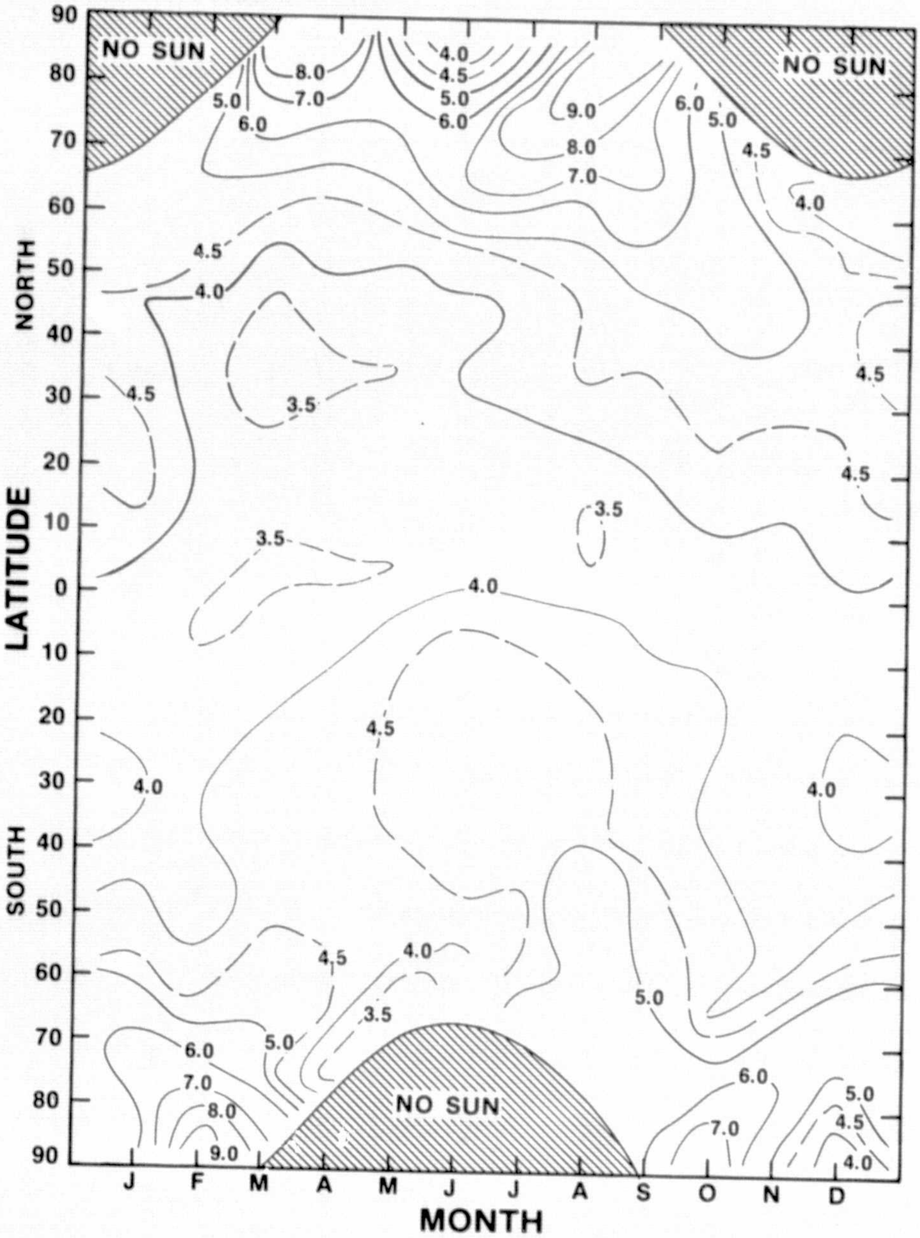

Figure 12. Reduction in Mean Monthly Solar Energy Absorbed in W/m^2 with Addition of Aerosol Layer of $\tau_{vis} = 0.1$

Table 9

Infrared Greenhouse Sensitivity

Model	Infrared Greenhouse Sensitivity $(W/m^2)/\tau_{vis}$	
	Clear Sky	Cloudy Sky
Tropical	14.8	7.5
Midlatitude Summer	13.8	6.9
Midlatitude Winter	8.6	3.6
Subarctic Summer	10.5	4.0
Subarctic Winter	5.6	1.8

An increase in the aerosol optical thickness of $\tau_{vis} = 0.1$, for example, would result in an increase in radiation trapped in the earth-atmosphere column under clear sky conditions of 1.5 W/m^2 in the tropics and 0.6 W/m^2 in the subarctic winter. Cloudiness may be taken into account by a weighting of the clear and cloudy sky results. This greenhouse moderation, when combined with solar depletion results in the distribution of net energy loss, $Q\Delta\alpha - \Delta I$ as shown in Figure 13 for $\tau_{vis} = 0.1$. Rather than use climatological cloudiness, the average of the clear and cloudy sky results has been used. Also, the greenhouse effect in spring and fall have been taken as intermediate between winter and summer.

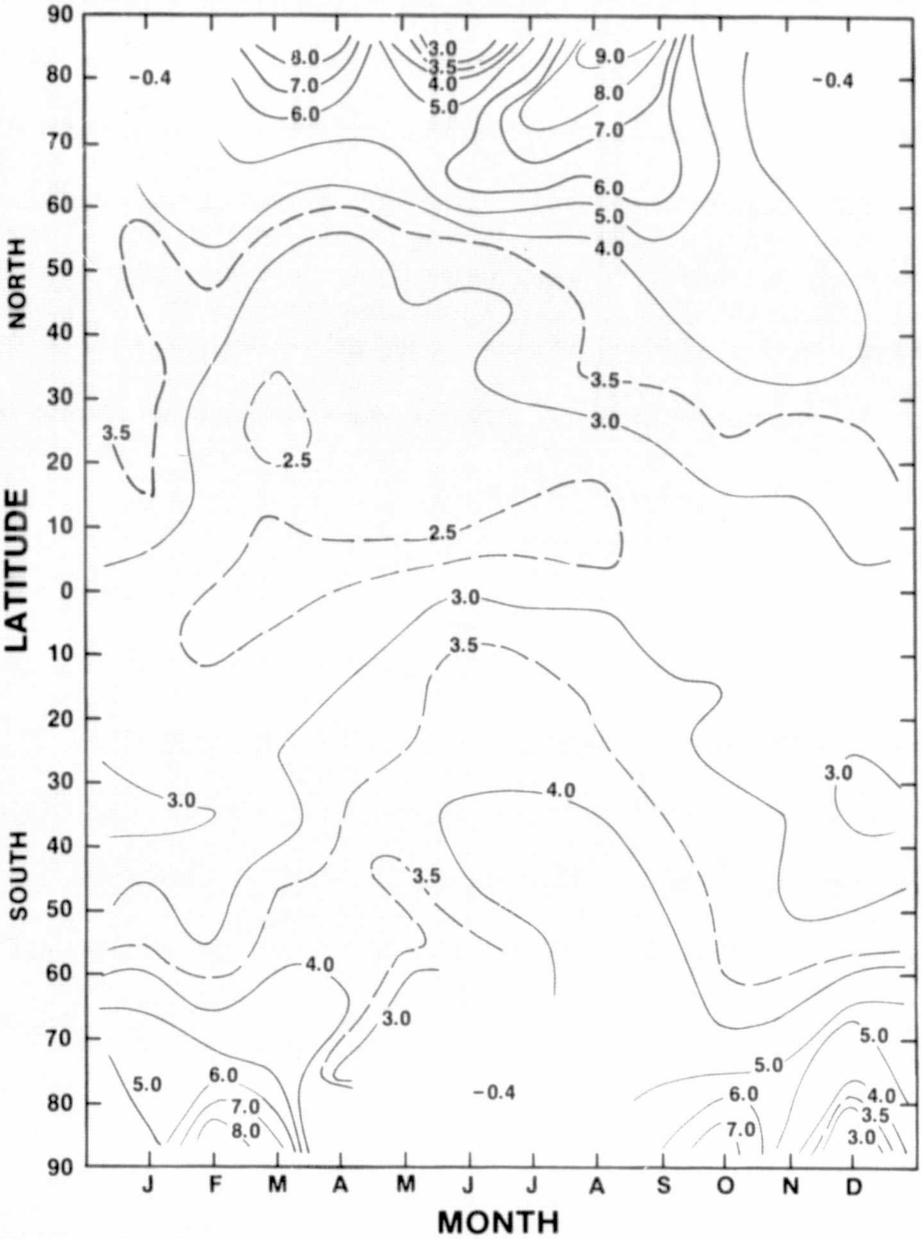

Figure 13. Reduction in the Zonal Radiation Balance in W/m^2 with Addition of Aerosol Layer of $\tau_{vis} = 0.1$

One observation from Figure 13 is that the presence of a stratospheric aerosol layer composed of 75% H_2SO_4 results in a loss of radiation absorbed within the earth-atmosphere system at all latitudes and seasons except the polar winter. The relationship between this net decrease in energy absorbed and mean atmospheric or surface temperature may be established through climate models. The maximum perturbation in the radiation balance occurs at high latitudes in the spring and fall whereas polar winters show a net gain in the radiation balance due to the increased greenhouse effect. Latitudes equatorward of 50° show a nearly uniform reduction in the radiation balance.

The magnitude of the change in the net radiation is only a small percentage of the range of typical values of the radiation balance. Monthly radiation balance over all latitudes have been presented by Ellis and Vonder Haar (1976) and values range from $-175\,W/m^2$ in the south polar winters to $+110\,W/m^2$ in the southern hemisphere tropics in summer. The uncertainty in mean monthly net radiation measurements ranges from 3 to $14\,W/m^2$ such that the computed values of the change in the radiation balance caused by the aerosol layer of $\tau_{vis} = 0.1$ are less than the uncertainty in the satellite derived data. It is unlikely that there will be a greater perturbation to the net radiation for extended periods of time following volcanic eruptions. Following the Agung eruption, $\tau_{vis} \approx 0.2$ in the Southern Hemisphere for a year (Volz, 1970) and even eruptions of greater magnitude will not alter the net radiation appreciably.

The perturbation in the radiation balance can also be expressed as a change in the effective black-body radiative temperature of the earth-atmosphere system. This change is given by

$$\Delta T = -\frac{Q\Delta\alpha - \Delta I}{4\sigma T^3} \tag{21}$$

where σ is the Stefan-Boltzmann constant, T the effective black-body radiative temperature of the earth-atmosphere system and $(Q\Delta\alpha - \Delta I)$ the change in the radiation balance. Figure 14 is a plot of ΔT in °K for $\tau_{vis} = 0.1$. The major features detected in the plot of radiation balance perturbation appear enhanced in this representation. It can be seen that the major radiative effect of the stratospheric aerosol layer occurs in the spring and fall when there is a pronounced change in the equator to pole radiative energy gradient. As the results pertain to the entire earth-atmosphere column, it is not possible to estimate the change in the diabatic heating at various levels of the atmosphere or estimate surface temperature changes. However, it appears from this analysis that a uniform layer of stratospheric aerosols would have only a small effect on the long term radiative regime equatorwards of 50°-60° if the change in turbidity corresponded to that caused by the Agung eruption. The localized radiative effect in the vicinity of the aerosol layer could still be considerable as discussed in Harshvardhan and Cess (1976).

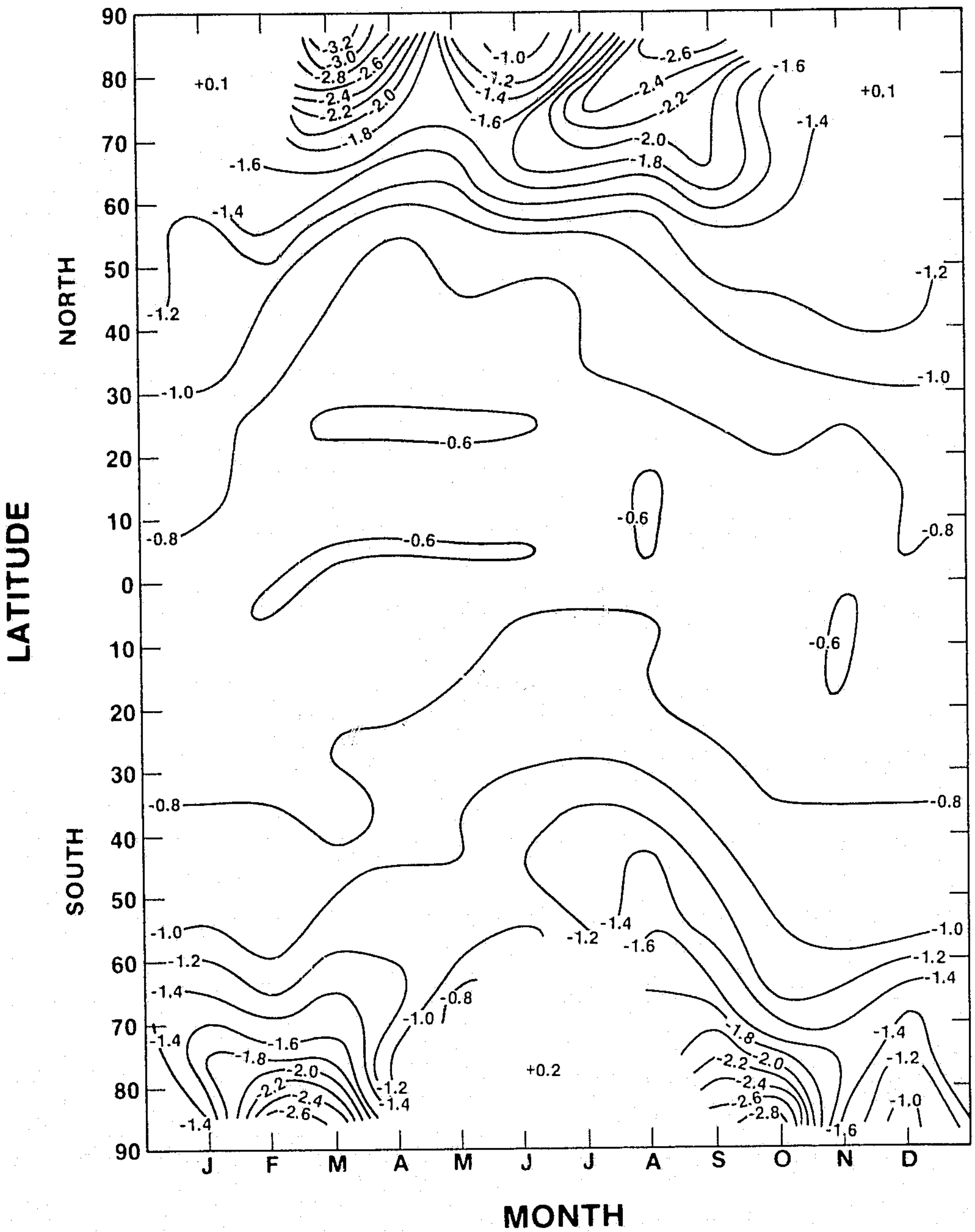

Figure 14. Change in the Effective Black-Body Radiative Temperature of the Earth-Atmosphere System in °K with Addition of Aerosol Layer of $\tau_{vis} = 0.1$

10. SUMMARY

The present study has examined the role of stratospheric aerosols in altering the radiation balance of the earth-atmosphere system. It has been confirmed that for an aerosol layer of 75% H_2SO_4 the dominant influence is an increased reflection of solar energy all over the globe except for the polar winters when there is no solar insolation. An important conclusion resulting from the albedo sensitivity computations is the necessity of including solar zenith angle effects in considering albedo enhancement. It was also pointed out that the separation of areas into cloud-covered and cloud-free is unnecessary in the calculation of the radiative effects of the reflecting layer. This enables the use of mean monthly planetary albedos obtained from satellite measurements to calculate the change in the radiation balance of each zonal belt caused by the presence of a stratospheric layer. The perturbation in the radiative balance may be used to simulate the radiative effect of a stratospheric aerosol layer in climate studies. Results indicate that the perturbation is strongest at high latitudes, particularly in the polar region, in the spring and fall.

REFERENCES

Braslau, N. and J. V. Dave, 1973: Effect of aerosols on the transfer of solar energy through realistic model atmospheres. Part II: partly absorbing aerosols. J. Appl. Meteor., Vol. 12, pp. 616-619.

Budyko, M. I., 1969: The effect of solar radiation variations on the climate of the earth. Tellus, Vol. 21, pp. 611-619.

__________, 1974: Climate and Life. Academic Press, New York, 508 pp.

Cadle, R. D. and G. W. Grams, 1975: Stratospheric aerosol particles and their optical properties. Rev. Geophys. Space Phys., Vol. 13, pp. 475-501.

Cess, R. D., 1976: Climate change: an appraisal of atmospheric feedback mechanisms employing zonal climatology. J. Atmos. Sci., Vol. 33, pp. 1831-1843.

Coakley, J. A. and P. Chylek, 1975: The two-stream approximation in radiative transfer: including the angle of the incident radiation. J. Atmos. Sci., Vol. 32, pp. 409-418.

Curran, R. J., R. Wexler and M. L. Nack, 1978: Albedo climatology analysis and the determination of fractional cloud cover. NASA Tech. Memo. 79576.

Dave, J. V. and N. Braslau, 1974: Effect of cloudiness on the transfer of solar energy through realisitc model atmospheres. Rept. RC 4869, IBM Thomas J. Watson Research Center, Yorktown Heights, N. Y.

__________ and __________, 1975: Effect of cloudiness on the transfer of solar energy through realistic model atmospheres. J. Appl. Meteor., Vol. 14, pp. 388-395.

Dyer, A. J. and B. B. Hicks, 1968: Global spread of volcanic dust from the Bali eruption of 1963. Quart. J. Roy. Meteor. Soc., Vol. 98, pp. 545-554.

Ellis, J. and T. H. Vonder Haar, 1976: Zonal average earth radiation budget measurements from satellites for climate studies. Atmos. Sci. Pap. 240, Colorado State University, Fort Collins, Co.

Hansen, J., 1969: Exact and approximate solutions for multiple scattering by cloudy and hazy planetary atmospheres. J. Atmos. Sci., Vol. 26, pp. 478-487.

Harshvardhan and R. D. Cess, 1976: Stratospheric aerosols: effect upon atmospheric temperature and global climate. Tellus, Vol. 28, pp. 1-10.

Herman, B. M., S. R. Browning, and R. Rabinoff, 1976: The change in earth-atmosphere albedo and radiational equilibrium temperatures due to stratospheric pollution. J. Appl. Meteor., Vol. 15, pp. 1057-1067.

Hofmann, D. J., J. M. Rosen, T. J. Pepin, and R. G. Pinnick, 1975: Stratospheric aerosol measurements I: time variations at Northern midlatitudes. J. Atmos. Sci.. Vol. 32, pp. 1446-1456.

Jacobowitz, H., W. L. Smith, H. B. Howell, F. W. Nagle, and J. R. Hickey, 1978: The first eighteen months of planetary radiation budget measurements from the Nimbus 6 ERB experiment. Preprints Third Conf. Atmospheric Radiation, Davis, Ca., Amer. Meteor. Soc., pp. 164-166.

Kondratyev, K. Ya. (Ed.), 1975: Radiation characteristics of the Atmosphere and the Earth's surface. NASA TTF-678, Amerind Publishing Co., New Delhi, 580 pp.

London, J., 1957: A study of the atmospheric heat balance. Report, Contract AF19(122)-165, College of Engineering, New York University.

Luther, F. M., 1976: Relative influence of stratospheric aerosols on solar and longwave radiative fluxes for a tropical atmosphere. J. Appl. Meteor., Vol. 15, pp. 951-955.

McClatchey, R. A., R. W. Fenn, J. E. A. Selby, F. E. Volz, and J. S. Garing, 1971: Optical properties of the atmosphere (rev.), Environ. Res. Pap. 54, Air Force Cambridge Res. Lab., Hanscom Air Force Base, Bedford, Mass.

Palmer, K. F. and D. Williams, 1975: Optical constants of sulfuric acid; application to the clouds of Venus? Appl. Optics, Vol. 14, pp. 208-219.

Pinnick, R. G., J. M. Rosen, and D. J. Hofmann, 1976: Stratospheric aerosol measurements III: optical model calculations. J. Atmos. Sci., Vol., 33, pp. 304-314.

Pollack, J. B., O. B. Toon, C. Sagan, A. Summers, B. Baldwin, and W. van Camp, 1976: Volcanic explosions and climatic change: a theoretical assessment. J. Geophys. Res., Vol. 81, pp. 1071-1083.

Rosen, J. M., 1971: The boiling point of stratospheric aerosols. J. Appl. Meteor., Vol. 10, pp. 1044-1046.

________, D. J. Hofmann, and J. Laby, 1975: Stratospheric aerosol measurements II: the worldwide distribution. J. Atmos. Sci., Vol. 32, pp. 1457-1462.

Russell, P. B. and R. D. Hake, Jr., 1977: The post-Fuego stratospheric aerosol: lidar measurements, with radiative and thermal implications. J. Atmos. Sci., Vol. 34, pp. 163-177.

Sellers, W. D., 1969: A global climatic model based on the energy balance of the earth-atmosphere system. J. Appl. Meteor., Vol. 8, pp. 392-400.

Shettle, E. P. and R. W. Fenn, 1976: Models of the atmospheric aerosols and their optical properties. AGARD Conference Proceedings No. 183 on Optical Propagation in the Atmosphere.

van Loon, H., 1972: Cloudiness and precipitation. Meteor. Monogr., No. 35, pp. 101-111.

Volz, F. E., 970: Atmospheric turbidity after the Agung eruption of 1963 and size distribution of the volcanic aerosol. J. Geophys. Res., Vol. 75, pp. 5185-5193.

Vonder Haar, T. H. and J. Ellis, 1975: Albedo of the cloud-free earth-atmosphere system. Preprints Second Conf. Atmospheric Radiation, Arlington, Va., Amer. Meteor. Soc., pp. 107-110.

Wiscombe, W. J., 1975: Solar radiation calculations for arctic summer stratus conditions. Climate of the Arctic, G. Weller and S. A. Bowling, Eds., Geophysical Institute, University of Alaska, pp. 245-254.

__________ and G. W. Grams, 1976: The backscattered fraction in two-stream approximations. J. Atmos. Sci., Vol. 33, pp. 2440-2451.